Evidence for two subpopulations of cerebrospinal-fluid contacting neurons with opposite GABAergic signaling in adult mouse spinal cord

Priscille Riondel, Nina Jurčić, Lourdes Mounien, Stéphanie Ibrahim, Jorge Ramirez-Franco, Sonia Stefanovic, Jérôme Trouslard, Nicolas Wanaverbecq, Riad Seddik

Evidence for two subpopulations of cerebrospinal-fluid contacting neurons with opposite GABAergic signaling in adult mouse spinal cord

Abbreviated Title: GABA signaling in spinal CSF-cNs of adult mouse

Priscille Riondel[1], Nina Jurčić[1], Lourdes Mounien[2,3], Stéphanie Ibrahim[2], Jorge Ramirez-Franco[1], Sonia Stefanovic[2], Jérôme Trouslard[1], Nicolas Wanaverbecq[1,*] and Riad Seddik[1,*]

[1] Institut de Neurosciences de la Timone, Aix-Marseille Université (AMU) & CNRS, UMR7289, Marseille, France.

[2] C2VN, Aix-Marseille Université, INRAE, INSERM, Marseille, France.

[3] PhenoMARS, Aix-Marseille Technology Platform, Marseille, France.

* RS and NW contributed equally to this work as Principal Investigators (PIs).

Correspondence should be addressed to:
riad.seddik@univ-amu.fr (R. SEDDIK) or
nicolas.wanaverbecq@univ-amu.fr (N. WANAVERBECQ).

Number of pages: 45
Number of figures: 8
Abstract: 242 words
Introduction: 649 words
Discussion: 1499 words

Conflict of interest

The authors declare no competing financial interests.

Acknowledgements

This research was supported by funding obtained from Aix-Marseille University (AMU), le Centre National pour la Recherche Scientifique (CNRS – INSB), and l'Agence Nationale pour la Recherche (ANR-16-CE92-0043-MotAct-CSF, NW). We gratefully thank Caroline Blanc-Tailleur and Anne Kastner for her assistance in immunohistochemistry experiments. We acknowledge the 'Institut de Neurosciences de la Timone (INT)' technical facilities for their support in the study (Neuro-Bio-Tools: Molecular Biology and Histology; INPHIM: confocal microscopy).

Abstract

Spinal cerebrospinal fluid-contacting neurons (CSF-cNs) form an evolutionary conserved bipolar cells population localized around the central canal of all vertebrates. CSF-cNs were shown to express molecular markers of neuronal immaturity into adulthood, however the impact of their incomplete maturation on the chloride (Cl^-) homeostasis as well as GABAergic signaling remain unknown. Using adult mice from both sexes, in situ hybridization revealed that a proportion of spinal CSF-cNs (18.3%) express the Na^+-K^+-Cl^- cotransporter 1 (NKCC1) allowing intracellular Cl^- accumulation. However, we did not find expression of the K^+-Cl^- cotransporter 2 (KCC2) responsible for Cl^- efflux in any CSF-cNs. The lack of KCC2 expression results in low Cl^- extrusion capacity in CSF-cNs under high Cl^- load in whole-cell patch-clamp. Using cell-attached patch-clamp allowing recordings with intact intracellular chloride concentration, we found that activation of ionotropic $GABA_A$ receptors induced both depolarizing and hyperpolarizing responses in CSF-cNs. Moreover, depolarizing GABA-responses can drive action potentials as well as intracellular calcium elevations by activating voltage-gated calcium channels. Blocking NKCC1 with bumetanide inhibited the GABA-induced calcium transients in CSF-cNs. Finally, we show that metabotropic $GABA_B$ receptors have no hyperpolarizing action on spinal CSF-cNs as their activation with baclofen did not mediate outward K^+ currents, presumably due to the lack of expression of G protein-coupled inwardly rectifying potassium (GIRK) channels. Together, these findings outline subpopulations of spinal CSF-cNs expressing inhibitory or excitatory $GABA_A$ receptors signaling. Excitatory GABA may promote maturation and integration of young CSF-cNs into the existing spinal circuit.

Significant Statement

Spinal CSF-contacting neurons (CSF-cNs) form a heterogeneous neural population with distinct maturation states in adult mice, but whether this reflects CSF-cNs with different GABAergic signaling remains unknown. Herein, we show that activation of $GABA_A$ receptors generates depolarization or hyperpolarization of CSF-cNs membrane potential in adult mouse spinal cord. Depolarizing GABA can trigger intracellular Ca^{2+} elevations through the activation of voltage-gated Ca^{2+} channels. Our results highlight a subpopulation of CSF-cNs in adult mice with depolarizing GABA that may promote their maturation and integration into the spinal cord.

Introduction

Chloride-permeable ionotropic $GABA_A$ receptors ($GABA_A$-Rs) mediate inhibition in adult brain, by generating chloride (Cl^-) entry into the cell and hence a hyperpolarization of the membrane potential. However, under conditions of intracellular Cl^- accumulation, $GABA_A$-Rs were shown to promote Cl^- outflow and thus depolarizing responses (Owens and Kriegstein, 2002). The intracellular Cl^- concentration in neurons is mainly determined by two Cl^- transporters, the K^+-Cl^- cotransporter 2 (KCC2) and the Na^+-K^+-Cl^- cotransporter 1 (NKCC1), whose expression/efficacy is developmentally regulated (Payne et al., 2003). In neuronal precursors and immature neurons, NKCC1 predominates and cotransports Cl^- ion into cells using the Na^+ gradient, thus allowing an increase of intracellular Cl^- concentration and depolarizing action of GABA. During neuronal maturation NKCC1 downregulates whereas KCC2 upregulates, leading to outward Cl^- directed transport. This allows a decline in the intracellular Cl^- concentration and a concomitant- shift in GABA responses from depolarization to hyperpolarization (Ben-Ari, 2002; Ben-Ari et al., 2012). However, there are few adult

neuronal populations in the central nervous system that retain immature-like functional characteristics under physiological conditions with the absence of KCC2 expression and depolarizing GABA transmission (Barthó et al., 2004; Haam et al., 2012; Sun et al., 2012)

Cerebrospinal fluid-contacting neurons (CSF-cNs) constitute a peculiar neuronal population present in brainstem and spinal cord of all vertebrates (Vígh et al., 2004; Djenoune et al., 2014). They lie at the interface between CSF and the parenchyma while extending a dendrite towards the central canal (CC), ending with a terminal protrusion or 'bud' in contact with the fluid (Stoeckel et al., 2003a; Marichal et al., 2009; Orts-Del'immagine et al., 2012). Based on their morphology and localization, it was proposed that CSF-cNs represent an intrinsic sensory module able to carry information from the CSF to spinal neuronal network (Fidelin et al., 2015; Böhm et al., 2016; Knafo et al., 2017; Gerstmann et al., 2022). Consistently, spinal CSF-cNs express selectively the polycystic kidney disease 2-like 1 (PKD2L1) channel, a sensory transduction protein sensitive to extracellular variation of pH, osmolarity and sensing CSF flow during spinal cord torsion (Orts-Del'immagine et al., 2012; Jalalvand et al., 2016; Orts-Del'Immagine et al., 2016; Sternberg et al., 2018). PKD2L1 are non-selective cationic channels and act as a potential generator in CSF-cNs for action potentials firing, suggesting a key role of PKD2L1 in tuning their excitability (Orts-Del'Immagine et al., 2016). CSF-cNs excitability is also adjusted by GABAergic synaptic inputs involving ionotropic $GABA_A$-Rs as well as G protein-coupled metabotropic $GABA_B$ receptors ($GABA_B$-Rs) (Orts-Del'immagine et al., 2012; Jurčić et al., 2019). Despite these apparent hallmarks of functionally mature neurons, CSF-cNs were also shown to express molecular markers of immaturity even into adulthood, such as the migrating and

neuronal shaping proteins doublecortin (DCX) and PSA- NCAM (polysialylated neuronal cell adhesion molecule) as well as the homeobox protein Nkx6.1 (Stoeckel et al., 2003b; Shechter et al., 2007; Orts-Del'immagine et al., 2014). This suggests that CSF-cNs persist in a prolonged immature state in the adult spinal cord, though the functional relevance of such immaturity has not been addressed. Specifically, the KCC2/NKCC1 expression properties are unknown in CSF-cNs of adult animals and their $GABA_A$ receptor-meditated transmission has, so far, only been studied with recording techniques that perturb the intracellular Cl^- concentration (Orts-Del'immagine et al., 2012).

In the present study, using *in situ* hybridization we show that a fraction of CSF-cNs in adult mouse spinal cord express the NKCC1 transporter whereas KCC2 mRNA was not detected in all CSF-cNs. Consistently, CSF-cNs have a lower Cl^- extrusion capacity when compared to mature $VGAT^+$ neurons of spinal dorsal horn. We further show that $GABA_A$-Rs activation induces hyperpolarizing responses but also depolarizations in a substantial proportion of CSF-cNs recorded in intact intracellular Cl^- conditions. Depolarizing $GABA_A$-Rs responses trigger action potentials and intracellular calcium elevations in CSF-cNs. Finally, we found that $GABA_B$-Rs do not mediate G protein-coupled inwardly rectifying potassium (GIRK) currents, further indicating that GABA cannot generate hyperpolarizations by acting on $GABA_B$-Rs in spinal CSF-cNs.

Materials and methods

Ethical approval

All experiments were conducted in conformity with the rules set by the EC Council Directive (2010/63/UE) and the French "Direction Départementale de la Protection des Populations des Bouches-du-Rhône (DDPP13)" (Project License Nr: APAFIS 17596; 2018111919329153. N.W. and License for the Use of Transgenic Animal Models Nr: DUO-5214). Protocols used agree with the rules set by the Comité d'Ethique de Marseille, our local Committee for Animal Care and Research. All animals were housed at constant temperature (21°C), in an enriched environment, under a standard 12h light-12h dark cycle, with food (pellet AO4, UAR, Villemoisson-sur-Orge, France) and water provided *ad libitum*. Every precaution was taken to reduce to the minimal the number of animals used and minimize animal stress during housing and prior to experiments.

Animals

Wildtype (C57BL/6J) and transgenic adult mice (7-10 weeks old) of both sexes were used in this study. Electrophysiological experiments were performed using wildtype C57BL/6J and (VGAT)-venus transgenic mice that express the fluorescent protein Venus under the control of the mouse VGAT (vesicular GABA transporter) promoter (generous gift of Dr Y. Yanagawa, Okazaki, Japan) (Wang et al., 2009). This allowed the identification of GABA/glycine ($VGAT^+$) mature neurons located in the spinal dorsal horn (see Results). For immunostainings experiments, PKD-tdTomato mice, used to identify spinal CSF-cNs, were generated by crossing PKD2L1-IRES-Cre transgenic

mice (generous gift from Dr E.R. Liman) with transgenic reporter Rosa26-loxP-stop-loxP-tdTomato mice (line Ai14 from The Jackson Laboratory). For RNAScope in situ hybridization experiments, we also used PKD-tdTomato mice but the tdTomato fluorescence was totally lost due to the protease treatment. Therefore, for identifying CSF-cNs we performed the hybridization of PKD2L1 transcripts (see below and the 'Results' section). Calcium imaging experiments were carried out in PKD-CCaMP6f mice obtained by breeding PKD2L1-IRES-Cre with transgenic reporter Rosa-GCaMP6f animals (line Ai95D supplied by The Jackson Laboratory), thus allowing the selective expression of the GCaMP6 fast variant calcium sensor in CSF-cNs (Madisen et al., 2015).

RNAScope fluorescent in situ hybridization

The detection of KCC2, NKCC1 and PKD2L1 mRNA was carried out with RNAScope Multiplex Fluorescent assays v2 (Advanced Cell Diagnostics) according to the manufacturer's instructions with minor modifications. Mice were transcardially perfused with ice-cold sterile PBS and the spinal cord was removed, then immediately embedded in OCT medium and frozen in liquid nitrogen. 20 μm thick coronal sections of the lumbar spinal cord were obtained using a cryostat (Microm HM550, Thermo Scientific), mounted onto SuperFrost Plus slides (Thermo Scientific) and stored at -80°C. Slides were postfixed in 4% paraformaldehyde at 4°C for 30 minutes and RNAScope Protease IV was applied for 20 minutes prior to hybridization. KCC2, NKCC1 and PKD2L1 in situ hybridization probes were provided by Advanced Cell Diagnostics (Cat No. 311901, 311911-C2 and 576471-C3, respectively). Hybridization products were visualized using TSA Vivid fluorophores (Advanced Cell Diagnostics).

TSA Vivid 520 (1:1000 dilution) was used for the KCC2 or NKCC1 probes and TSA Vivid 570 (1:1000) was used for the PKD2L1 probe. Sections were counterstained with DAPI, mounted with ProLong Gold (Life Technologies) and visualized with a confocal LSM 700 or Axio Zoom.V16 Zeiss microscope. Acquired images were subsequently analyzed with ImageJ 1.53s software (NIH).

Immunohistochemistry

Adult PKD-tdTomato mice were first (30 minutes prior the procedure) injected with the non-steroidal anti-inflammatory Metacam (5mg/kg) and subsequently anesthetized with intraperitoneal administration of 100 mg/kg ketamine (Carros, France) and 10 mg/kg xylazine (Puteau, France). Before skin incisions, the local antalgic Lurocaine (5mg/kg) was injected subcutaneously. Animals were then transcardially perfused with 0.1 M PBS followed by 4% paraformaldehyde (PFA; Sigma-Aldrich) and tissues were immediately removed, post-fixed for 1 h in PBS 4% PFA at room temperature then transferred in PBS. The lumbar region of spinal cord was embedded in low-melting point agarose (4% solution, in PBS) and sectioned into 40 µm thick coronal sections with a vibrating microtome (Leica VT1000S). Free-floating sections were permeabilized for 1 h at room temperature using PBS with 0.2% Triton X100 (Sigma) and 3% BSA (bovine serum albumin). Sections were then blocked for 45 minutes at room temperature with PBS containing 1% NGS (normal goat serum) and 3% BSA followed by overnight incubation at room temperature with rabbit anti-KCC2 IgG (1:1000 dilution; #07-432, Merck-Millipore) (Yassin *et al.*, 2014). After primary antibody incubation, tissues were washed with PBS and incubated for 2 h with secondary antibodies conjugated to AlexaFluor 488 (1:400; Invitrogen). Sections were

then rinsed with PBS, counterstained with DAPI (1:1000; Invitrogen) and mounted on gelatine-coated slides and coverslipped with home-made mowiol mounting medium for confocal microscopy. Confocal images were captured with a Zeiss LSM 700 laser scanning microscope and then processed with ImageJ 1.53s software (NIH). For the fluorescence profile analysis, the straight-line tool of ImageJ was used to trace lines along the cell perimeter. Raw intensity values were then collected, normalized to the maximum value, and plotted as a function of distance.

Acute spinal cord slice preparation

Coronal spinal cord slices were prepared as previously described (Gerstmann et al., 2022). Briefly, adult wildtype or transgenic mice were anesthetized with the ketamine-xylazine mixture and perfused intracardially with an ice-cold (0-4°C), oxygenated (95% O_2/5% CO_2) and low calcium/high magnesium cutting solution containing (in mM): NaCl 75, $NaHCO_3$ 33, NaH_2PO_4 1.25, KCl 3, $CaCl_2$ 0.5, $MgSO_4$ 7, glucose 15, sucrose 58, ascorbic acid 2, Na-pyruvate 2, *myo*-Inositol 3 (pH 7.3-7.4 and osmolality of 300-310 mosmole.kg^{-1}). Following laminectomy and spinal cord dissection, lumbar spinal cord slices (250 µm thick) were cut with a vibratome (Leica VT1000S) in ice-cold cutting solution saturated with 95% O_2-5% CO_2. Slices were subsequently transferred to a holding chamber and incubated at 35° C for 15-20 minutes in oxygenated artificial CSF (aCSF) containing (in mM): NaCl 115, $NaHCO_3$ 26, NaH_2PO_4 1.25, KCl 3, $CaCl_2$ 2, $MgSO_4$ 2, glucose 15, ascorbic acid 2, Na-pyruvate 2, *myo*-Inositol 3 (pH 7.3-7.4 and osmolality of 300-310 mosmole.kg^{-1}) and then kept at room temperature before recordings.

Electrophysiology

Slices were placed in a recording chamber and superfused with oxygenated aCSF (1.5-2.0 mL/min) maintained at 30°C by an in-line peltier heater (Scientifica). Neurons around the central canal were visualized under infrared illumination with a 40x objective and oblique optics mounted on a Scientifica SliceScope Pro 1000. Data were acquired with an Axopatch 200A patch-clamp amplifier (Molecular Devices Inc.), low-pass filtered at 2 KHz and digitized at 10-20 KHz using a Digidata 1322A interface driven by pClamp 10 software (Molecular Devices). Patch pipettes (4-6 MΩ) were pulled from borosilicate glass capillaries (Harvard Apparatus) using the vertical PC-100 puller (Narishige International Ltd) and filled with an internal solution supplemented with 10 μM of the fluorescent dye AlexaFluor 594 (Invitrogen). In all experiments, CSF-cNs identity was confirmed by the recording of PKD2L1 channel activity as well as the visualization of the dendritic protrusion (or bud) after whole-cell dialysis with Alexa 594.

GABA reversal potentials measurement

$GABA_A$ current reversal potentials (E_{GABA}) were determined with whole-cell voltage-clamp recordings using electrodes filled with a solution containing (in mM): K-Gluconate 119, KCl 21, NaCl 4, HEPES 5, $MgCl_2$ 2, EGTA 1.1, Na_2-ATP 2, Creatine-Phosphate 5, Na_3GTP 0.6 (adjusted to pH 7.35 with KOH). Currents were evoked by brief (30 ms) puffs of GABA (1 mM) from a patch pipette at intervals of 10 s between applications and in the presence of DNQX (20 μM) and strychnine (1 μM) to block AMPA/kainate glutamatergic and glycinergic synaptic transmission, respectively. GABA I-V curves were obtained by averaging three consecutive responses for each voltage step and plotting the peak current amplitude as a function of the membrane

potential. Experimental data points were fitted with linear regression and E_{GABA} was determined as the x-intercept of the linear fit. Membrane potentials were corrected offline for liquid junction potential (10 mV). Theoretical E_{GABA} was calculated with the Hodgkin-Katz-Goldman equation assuming a permeability ratio between Cl^- and HCO_3^- anions of 0.25 (Bormann et al., 1987; Kaila, 1994).

Cell-attached recordings

CSF-cNs membrane potential (V_m) were estimated by measuring the reversal potential of K^+ currents in cell-attached patches, as described previously (Fricker et al., 1999; Verheugen et al., 1999) with patch pipettes filled with a high K^+ solution containing (in mM): K-Gluconate 140, NaCl 4, HEPES 5, $MgCl_2$ 2, EGTA 1.1, Na_2-ATP 2, Creatine-Phosphate 5, Na_3GTP 0.6 (adjusted to pH 7.35 with 4 mM KOH). In these conditions, the $[K^+]$ in the pipette solution is close to the estimated intracellular $[K^+]$ in other cell types (Hille, 1992) so that the equilibrium potential for K^+ (E_K) across the patch would be around 0 mV and K^+ currents reverse when the pipette potential (V_{pip}) cancels V_m out. Therefore, the neuron holding potential ($-V_{pip}$) at which K^+ currents reverse gives a direct and non-invasive quantitative measure of V_m (at K^+ reversal, $V_{patch} = V_m - V_{pip} \approx 0$ mV). Voltage-gated K^+ channels were activated with voltage ramps (-140 to +200 mV for 100 ms) applied every 1 s, in control and during pressure application of GABA (1 mM, 10 s duration). K^+ currents were recorded in the presence of TTX (0.5 μM), DNQX (20 μM) and strychnine (1 μM). E_K was measured from the intersection between the K^+ current and the fit to the linear component.

The effect of GABA on CSF-cNs firing activity was investigated with tight-seal cell-attached recordings in voltage-clamp mode by adjusting the command potential to

result in a holding current of 0 pA (Perkins, 2006). Action potential (AP) currents were recorded in control and during pressure application of GABA (1mM, 5 s duration). In each cell and before AP recording, the effect of GABA on CSF-cNs membrane potential (depolarizing or hyperpolarizing) was assessed with cell-attached current-clamp recordings in tight-seal configuration and with pressure application of the agonist (1 mM, 5 s duration; see Results). Voltage-clamp and current-clamp cell-attached recording were performed with patch pipettes filled with K-gluconate based internal solution.

Recording of inwardly-rectifying (GIRK/kir3) potassium currents

Postsynaptic GIRK-type K^+ currents were recorded in voltage-clamp whole-cell configuration with patch electrodes filled with a solution containing (in mM): 140 K-gluconate, 4 NaCl, 5 HEPES, 2 $MgCl_2$, 1.1 EGTA, 2 Na_2ATP, 5 Na_2-phosphocreatine, 0.6 Na_3GTP (adjusted to pH 7.35 with KOH). GIRK currents were evoked by bath application of $GABA_B$-Rs selective agonist baclofen (100 μM) or the potent activator of GIRK1/2 channels ML297 (VU0456810, 100 μM) (Kaufmann et al., 2013) at a holding potential of -50 mV and in the presence of antagonists DNQX (10 μM) and strychnine (1 μM).

Calcium imaging

CSF-cNs selectively expressing the fluorescent probe GCaMP6f-lck (a membrane bound form of GCaMP6f) were illuminated by light through an 490/30 nm (peak/bandwidth) excitation filter using the CoolLED epifluorescence system (p1 PrecisExcite). Emitted light was bandpass filtered at 535/30 nm and collected with the

HQ2 CoolSnap CCD camera (standard mode at 10 MHz and Gain 1, Photometrics) connected to a PC through a frame grabber (CoolSNAP LVDS interface card, Photometrics) and controlled by the MetaView software (Molecular Devices Inc.). Images were acquired in time lapse mode with a 2x2 binning for 100 ms at 2 Hz for 70 s period (141 images). For each image, a region of interest (ROI) was drawn over the CSF-cN soma as well as the background and the average intensity of the fluorescence in these two ROIs was calculated. Subsequently, the background fluorescence intensity was subtracted from the somatic data to compute the net fluorescence (F) and data were expressed as the change of fluorescence relative to basal fluorescence ($(F- F_0)/F_0$ or $\Delta F/F_0$). Modifications in intracellular Ca^{2+} concentration ($[Ca^{2+}]_i$) were evoked at room temperature by pressure application of GABA (1 mM, 10 s duration) or high-potassium aCSF (20 mM, 10 s duration) in the presence of DNQX (20 μM), strychnine (1 μM) and the selective antagonist CGP54626 (10 μM) of $GABA_B$-Rs to prevent their inhibitory effect on voltage-gated calcium channels (Jurčić et al., 2019). In experiments with calcium-free aCSF (0-Ca^{2+}), slices were perfused with external solution containing (in mM): NaCl 115, $NaHCO_3$ 26, NaH_2PO_4 1.25, KCl 3, $MgSO_4$ 4, glucose 15, ascorbic acid 2, Na-pyruvate 2, *myo*-Inositol 3, EGTA 0.2.

Data analysis and statistics

Electrophysiological data were analyzed using Clampfit 10 (Molecular Devices Inc.), Excel 2016 (Microsoft) and Prism 10 software (GraphPad). Data were expressed as mean ± SD in text and represented as box-whisker plot using the Tukey's method with Prism 10 software. The box plot represents the distribution of data as a box, with the median as a central line and the hinges as the edges of the box (lower and upper hinges

corresponding to the 25th and 75th percentiles, respectively). The upper whisker extends to the largest value in the data set that does not exceed 1.5 times the interquartile range (IQR) plus the 75th percentile (where IQR is the difference between the 25th and the 75th percentiles). The lower whisker extends to the smallest value higher than the 25th percentile minus 1.5 times IQR. Data beyond the end of the whiskers are called outliers and are plotted individually as circles. Throughout the manuscript, "n" and "N" refer to the number of cells and mice exanimated, respectively. All data were tested for normal distribution using the Shapiro-Wilk test with Prism 10 and the result determined the use of parametric or nonparametric statistical tests indicated in the Results section. Fisher's exact test was used to compare 2 × 2 contingency tables. Statistical tests were performed with Prism 10 and differences were considered significant when $p < 0.05$.

Reagents

All reagents were purchased from Sigma-Aldrich except otherwise stated. Tetrodotoxin (TTX) was from Alomone Labs. 6,7-dinitroquinoxaline-2,3-dione disodium salt (DNQX) and ML297 (VU0456810) were from Abcam Biochemicals. (R)-baclofen, gabazine (SR 95531), CGP54626 and VU0463271 were from Tocris Bio-techne. All drugs were diluted in aCSF to their final concentration immediately prior to use.

Results

NKCC1 transporters are expressed in spinal CSF-cNs of adult mice but not KCC2

CSF-cNs were shown to persist in an immature state in adult spinal cord (Kútna et al., 2014; Orts-Del'immagine et al., 2014). Moreover, it is well known that developing neurons of the CNS lack KCC2 while they highly express NKCC1 (Rivera et al., 1999; Blaesse et al., 2009). Therefore, we first investigated the expression of NKCC1 and

KCC2 in adult spinal CSF-cNs by comparing the distribution of their mRNAs with fluorescent *in situ* hybridization (RNAScope). KCC2 and NKCC1 mRNAs expression were analyzed in CSF-cNs identified by the hybridization of PKD2L1 transcripts as the channel was shown to selectively express in CSF-cNs (Orts-Del'Immagine et al., 2014). We found that 18.3 ± 13.4% of $PKD2L1^+$ CSF-cNs contained transcripts for NKCC1 (20 $NKCC1^+$ cells out of 98 $PKD2L1^+$ CSF-cNs, N = 2; Fig. 1A, B, C and G). In contrast, KCC2 mRNAs were not detected in all analyzed $PKD2L1^+$ CSF-cNs (n = 87, N = 2; Fig. 1D, E, F and G) whereas KCC2 mRNA signal is found in neurons lacking PKD2L1 and surrounding the central canal (arrowheads, Fig 1E and F). As controls and for validating the specificity of the RNAScope procedure, *in situ* hybridization of KCC2 and NKCC1 was performed in the hippocampal CA1 region and choroid plexus epithelial cells that were shown to highly express KCC2 and NKCC1, respectively (Kurki et al., 2023). Strong KCC2 mRNA signal was detected in CA1 neurons (Fig. 1Ha) while only few particles representing NKCC1 were observed in the hippocampal CA1 region, as previously described (arrowhead, Fig. 1Hb) (Kurki et al., 2023). On the other hand, and as expected (Kurki et al., 2023), we found a high expression of NKCC1 (Fig. Ia) but no KCC2 mRNAs (Fig. Ib) in choroid plexus epithelial cells.

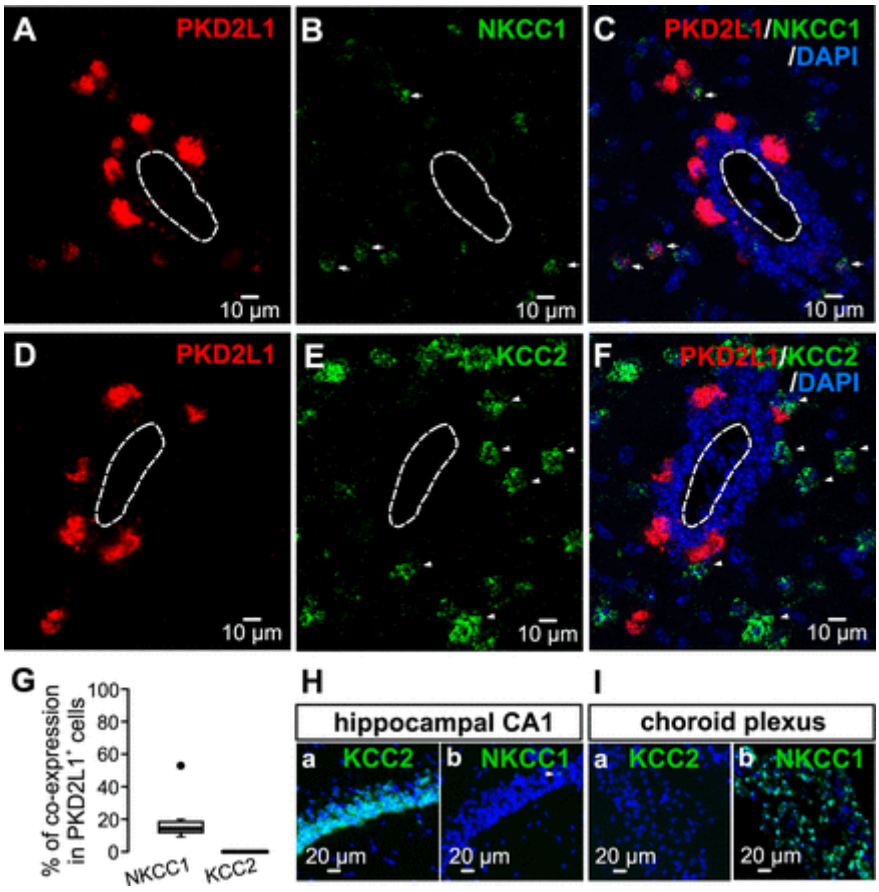

Figure 1.

CSF-cNs of adult spinal cord express NKCC1 but not KCC2 mRNAs. ***A–C***, Confocal images showing in CSF-cNs the expression of NKCC1 mRNAs (arrows, green panel ***B***) following fluorescence in situ hybridization (RNAscope). CSF-cNs were identified by the presence of PKD2L1 mRNA transcripts (red, panel ***A***; merged image in panel ***C***). ***D–F***, In situ hybridization showed no expression of KCC2 (green, panel ***E***) in PKD2L1^{+} CSF-cNs (red, panel ***D***; merged image in panel ***F***). However, we found a strong KCC2 mRNA signal in neurons negative for PKD2L1 and surrounding the CC (arrowheads, panel ***E***; merged image in panel ***F***). Cell nuclei were counterstained with DAPI (blue, panel ***C***,***F***). White dashed lines delineate the CC. ***G***, Box-and-whisker plot showing the percentage of NKCC1 and KCC2 coexpression in PKD2L1^{+} CSF-cNs (NKCC1, 20 cells out of 98 PKD2L1^{+} cells; KCC2, 0 cells out of 87 PKD2L1^{+} cells). ***H***, Hippocampal CA1 region shows a strong KCC2 (***a***) but sparse NKCC1 mRNA signal (***b***, arrowhead), thus confirming the specificity of in situ hybridization experiments. ***I***, The absence of KCC2 expression (***a***) together with the strong NKCC1 mRNA signal (***b***) in choroid plexus epithelial cells provides additional controls for the RNAscope procedure.

We further confirmed the absence of KCC2 expression in CSF-cNs with immunostainings and using transgenic PKD-tdTomato mice expressing the fluorescent protein tdTomato in CSF-cNs for their identification. We found no detectable KCC2 immunostainings in all analyzed tdTomato^{+} CSF-cNs (n = 96, N = 3; arrows, Fig. 2A-D; Fig. 2E, F, H and M) whereas KCC2 immunoreactivity was observed in the plasmalemmal region of neurons surrounding the CC and lacking tdTomato expression (arrowheads, Fig. 2B-D; Fig. 2I, J, L and N; N = 3). As an additional positive control, we show that dorsal horn (DH) neurons also express membrane immunostaining for KCC2, as previously reported (Ferrini et al., 2020) (Figure 2O and P).

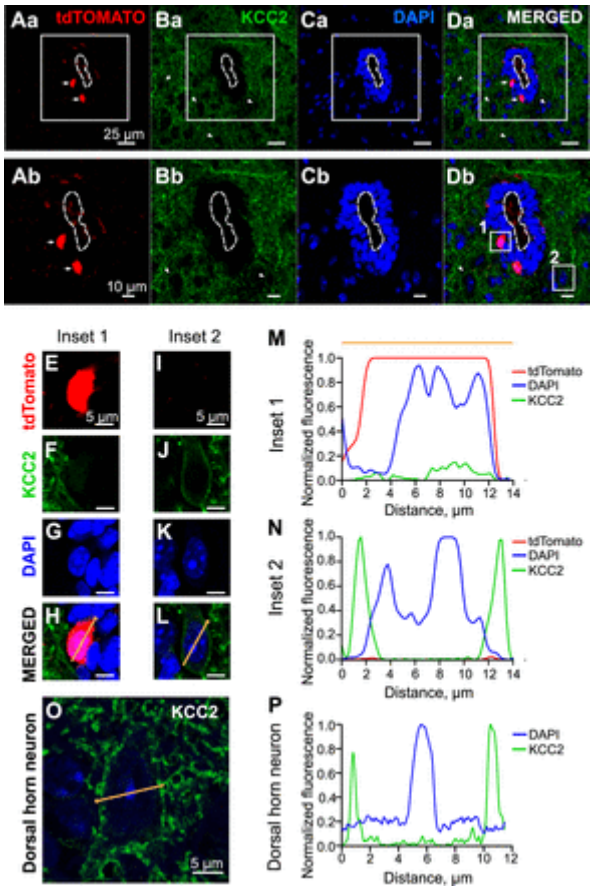
Aa tdTOMATO
Ba KCC2
Ca DAPI
Da MERGED
25 µm
Ab
Bb
Cb
Db
10 µm
1
2
Inset 1
Inset 2
tdTomato
KCC2
DAPI
MERGED
E
I
F
J
G
K
H
L
5 µm
M
Inset 1
N
Inset 2
Normalized fluorescence
Distance, µm
tdTomato
DAPI
KCC2
O
KCC2
Dorsal horn neuron
P
Dorsal horn neuron

Figure 2.

The absence of immunostaining for KCC2 in spinal CSF-cNs. A–D, Confocal microscopy images showing no detectable KCC2 immunostaining (green, panels Ba and Bb) in adult CSF-cNs identified by their selective tdTomato expression (red, arrows in panels Aa and Ab; merged images in panels Da and Db). Panels Ab–Db show higher magnification of the boxed regions indicated in panels Aa–Da. However, neurons lacking tdTomato expression (non-CSF–cNs) show plasmalemmal immunostaining for KCC2 (arrowheads, panels Ba, Bb, Da, and Db). Cell nuclei were counterstained with DAPI (blue, panels Ca and Cb; merged images in panels Da and Db). Panels Ab–Db are images at higher magnification from panels Aa–Da (white box). The CC is delineated by white dashed lines. E–L, Expanded view of the tdTomato+ CSF-cNs (red, E–H) and non-CSF–contacting tdTomato− neurons (I–L) highlighted in Insets 1 and 2 of the merged picture in Db. Plasma membrane immunostaining for KCC2 (green) is detected in non-CSF–cNs (panels I,J; merged image in panel L) but not in CSF-cNs (panels E,F; merged image in panel H). Nuclei were counterstained with DAPI (blue, panels G,K; merged images in panels H,L). M–N, Fluorescent intensity line profile analysis for tdTomato (red), KCC2 (green), and DAPI (blue) of cells illustrated in Insets 1 and 2. No KCC2 fluorescence is detected in the tdTomato+ CSF-cN (M), whereas the fluorescence profile of KCC2 in the non-CSF–contacting tdTomato− neuron (N) indicates plasma membrane expression of KCC2. Intensity values for KCC2 and the tdTomato were normalized to the maximal value obtained from the non-CSF–cN and CSF-cN, respectively. O–P, Confocal image (O) and fluorescence intensity line profile analysis (P) showing KCC2 immunoreactivity in a DH neuron. The start points (0 μm) for the line profiles on the graphs in panels M, N, and P are illustrated by the orange dots of the line drawn on images H, L, and O.

Altogether, these data indicate a lack of KCC2 in spinal CSF-cNs of adult mice while NKCC1 is present in a fraction of neurons, which may result in Cl^- accumulation and depolarizing GABA in these cells.

Low Cl^- extrusion capacity in spinal CSF-cNs

KCC2 deficiency may involve lower Cl^- extrusion capacity in CSF-cNs. To test this hypothesis, we compared the Cl^- extrusion capability between CSF-cNs and dorsal horn (DH) $VGAT^+$ (GABA/glycine) neurons expected to have active KCC2-dependant Cl^- extrusion (Ferrini et al., 2020). Cl^- extrusion capacity was assessed under constant Cl^-

load by recording CSF-cNs and DH $VGAT^+$ neurons in whole-cell configuration with high Cl^- concentration in the recording pipette (29 mM, Fig. 3A). Under these conditions and according to the Goldman-Hodgkin-Katz (GHK) equation, the theoretical value of the reversal potential of $GABA_A$ receptor-mediated currents (E_{GABA}) is -38 mV. GABA-mediated currents were elicited by pressure applications of GABA (1 mM, 30 ms) and recorded at different holding potentials to generate the IV curve and determine E_{GABA} (see Methods). The E_{GABA} determined experimentally was then compared to the calculated one. As previously described, a more negative imposed E_{GABA} compared to the calculated value reveals active Cl^- extrusion (Cordero-Erausquin et al., 2005; Schmidt et al., 2018; Ferrini et al., 2020). Using (VGAT)-venus transgenic mice allowing the expression of the venus protein in $VGAT^+$ neurons (Fig. 3B), we recorded dorsal horn (DH) $VGAT^+$ neurons and found they have an experimental value of E_{GABA} (-47.8 ± 13 mV, n = 19, N = 4) hyperpolarized from the calculated $E_{GABA,}$ indicating effective Cl^- extrusion (Fig. 3C, E and F). In CSF-cNs lacking KCC2, E_{GABA} was significantly more depolarized (-30.5 ± 3.4 mV, n = 18, N = 4; Fig. 3D and E) compared to DH $VGAT^+$ neurons ($p = 1.6 \times 10^{-5}$, unpaired Student's t-test; Fig. 3F) and close to the calculated E_{GABA}, hence indicating a weaker extrusion capacity in CSF-cNs. GABA-induced currents at the different holding potentials were fully inhibited (from -60 to +20 mV; n = 4, N = 2) in CSF-cNs perfused with the $GABA_A$ receptors antagonists gabazine (GBZ, 10 μM) and picrotoxin (PTX, 100 μM) (Fig 3Ga, Gb and H), supporting that the recorded currents were solely mediated by $GABA_A$ receptors. Moreover, pressure application of external solution without GABA (aCSF) did not change the holding current, showing that in our conditions pressure application does not mediate mechanical responses in CSF-cNs (n = 8, N = 2; Fig. 3I).

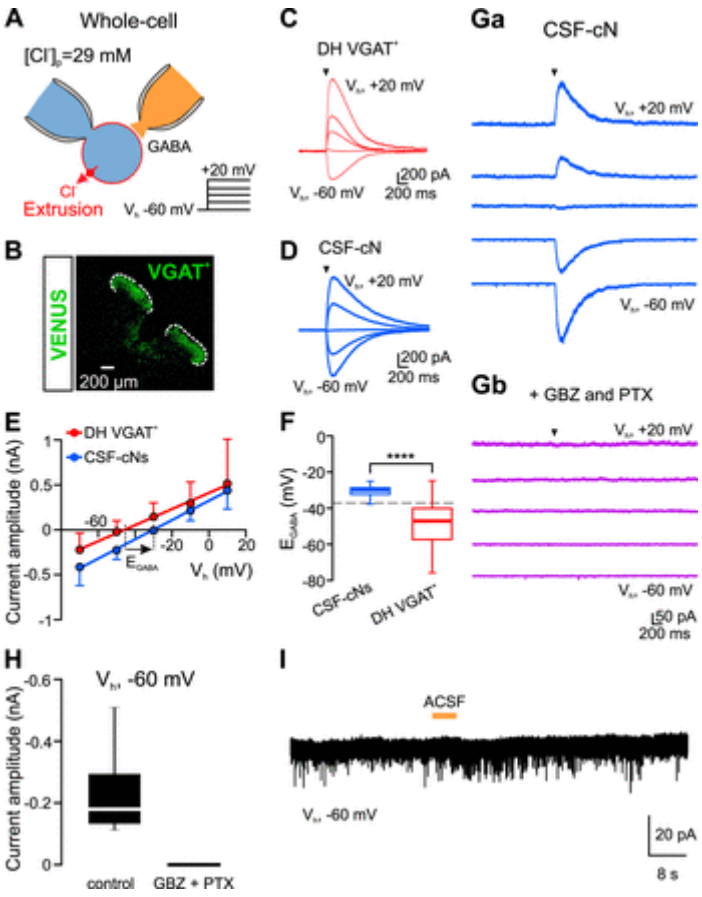
A
Whole-cell
[Cl⁻]ᵢ=29 mM
GABA
Cl⁻
Extrusion
+20 mV
Vₕ -60 mV
B
VENUS
VGAT⁺
200 µm
C
DH VGAT⁺
Vₕ +20 mV
200 pA
200 ms
Vₕ -60 mV
D
CSF-cN
Vₕ +20 mV
200 pA
200 ms
Vₕ -60 mV
Ga
CSF-cN
Vₕ +20 mV
Vₕ -60 mV
Gb
+ GBZ and PTX
Vₕ +20 mV
Vₕ -60 mV
50 pA
200 ms
E
DH VGAT⁺
CSF-cNs
Current amplitude (nA)
-60
E_GABA
Vₕ (mV)
F
E_GABA (mV)
****
CSF-cNs
DH VGAT⁺
H
Vₕ -60 mV
Current amplitude (nA)
control
GBZ + PTX
I
ACSF
Vₕ -60 mV
20 pA
8 s

Figure 3.

Adult spinal cord CSF-cNs have low Cl− extrusion capacity. A, Cl− extrusion measurements were performed in whole-cell configuration by recording GABAA-R–mediated currents in cells maintained at different holding potentials (Vh, from −60 mV to +20 mV; steps of +20 mV) and with a pipette solution containing high Cl− (29 mM). B, Confocal image showing VGAT+ (GABA/glycine) neurons in the spinal DH (white dash line) expressing the Venus fluorescent protein. C,D, Representative averaged current traces evoked by GABA pressure applications (1 mM, 30 ms duration, arrowheads) recorded in one DH VGAT+ neuron (C, red traces) and one CSF-cN (D, blue traces) in the presence of DNQX (20 μM) and strychnine (1 μM). E, Mean GABA I–V curves recorded from DH VGAT+ neurons (red) and CSF-cNs (blue). In CSF-cNs, EGABA (−33.1 mV; R2 = 0.8; defined by the x-intercept of the linear fit, dashed line) is shifted to more positive values compared with DH VGAT+ neurons (−45.9 mV; R2 = 0.5). Membrane potentials were corrected for liquid junction potential (10 mV). F, Box-and-whisker plot for EGABA measured in CSF-cNs (−30.5 ± 3.4 mV; n = 18; N = 4) and DH VGAT+ neurons (−47.8 ± 13 mV; n = 19; N = 4). EGABA in CSF-cNs was significantly more depolarized compared with DH neurons (****p = 1.6 × 10−5; unpaired Student's t test). The gray dashed line shows the theoretical EGABA (−38 mV) calculated with GHK equation. G, Representative traces showing GABAA-R currents evoked by pressure applications of GABA (arrowheads, 1 mM for 30 ms) in one representative CSF-cN maintained at different holding potentials in control (a) and in the presence of the GABAA-R antagonists (b), GBZ (10 μM) and PTX (100 μM). H, Box-and-whisker plot of GABA currents amplitude recorded at −60 mV showing that currents are fully abolished in the presence of GBZ and PTX (control, −231.3 ± 126.5 pA; n = 10; N = 3). I, Pressure application of external solution without GABA (aCSF) did not change the holding current in CSF-cNs held at −60 mV.

Consistent with an active Cl^- extrusion in DH $VGAT^+$ neurons, bath application of the potent and selective KCC2 inhibitor VU0463271 (10 μM) shifted E_{GABA} to more positive values in these neurons (control: -41.5 ± 8.3 mV; VU0463271: -31.6 ± 6.5 mV, n = 5, N = 4; p = 0.0014, Student's two-tailed paired t-test; Fig. 4A, B and C). In contrast, VU0463271 had no effect on E_{GABA} measured in CSF-cNs (control: -30,8 ± 2.9 mV; VU0463271: -27.6 ± 7.1 mV, n = 8, N = 4; p = 0.1, Student's two-tailed paired t-test; Fig. 4D, E and F).

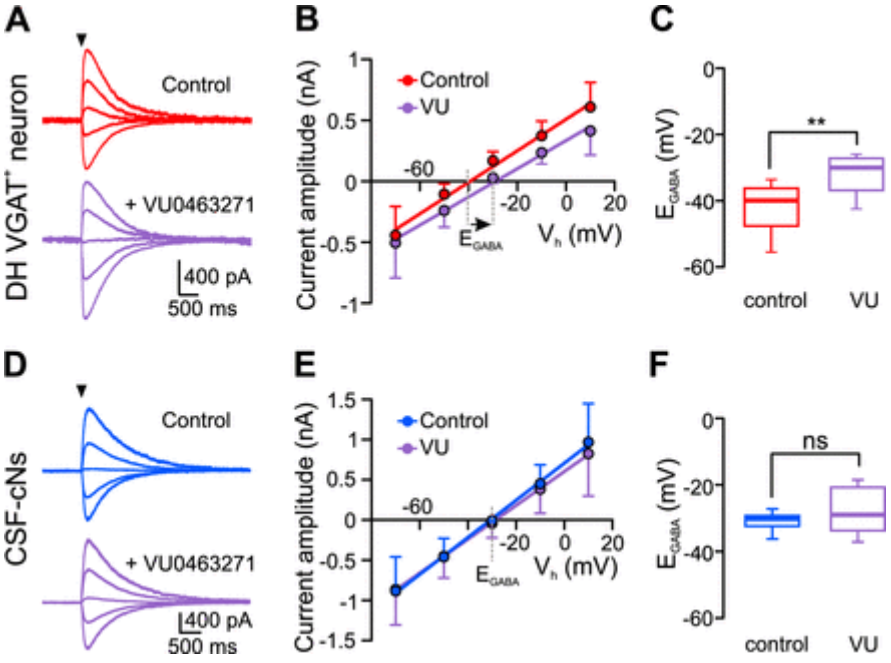

Figure 4.

Selective KCC2 inhibition shifts the EGABA in DH VGAT+ neurons but not in CSF-cNs. Representative current traces (A,D) and mean I–V plots (B,E) for GABA-induced currents recorded in DH VGAT+ neurons (A,B) and CSF-cNs (D,E) in control (red and blue traces and circles for DH VGAT+ and CSF-cNs, respectively) and in the presence of VU0463271 (VU, 10 µM; purple traces and circles), a KCC2-specific inhibitor. Currents were elicited with GABA pressure application (1 mM for 30 ms; arrowheads in A and D) in the presence of DNQX (20 µM), strychnine (1 µM), and BTN (20 µM). In DH VGAT+ neurons, EGABA obtained in the presence of VU0463271 is shifted to more positive values compared with control (B, control, EGABA = −39.4 mV; R2 = 0.9; VU, EGABA = −28.9 mV; R2 = 0.9; x-intercept of the linear fit), while it remained unchanged in CSF-cNs (E, control, EGABA = −30.6 mV; R2 = 0.9; VU, EGABA = −28.6 mV; R2 = 0.9). The gray dashed lines in B and E indicate EGABA measured in control and in the presence of VU. C,F, Summary box-and-whisker plots of EGABA from DH VGAT+ neurons (red) and CSF-cNs (blue) in control and in the presence of VU0463271 (purple) conditions (DH VGAT+ neurons, control, −41.5 ± 8.3 mV; VU, −31.6 ± 6.5 mV; n = 5; N = 4; **p = 0.0014; Student's two-tailed paired t test; and in CSF-cNs, control, −30.8 ± 2.9 mV; VU, −27.6 ± 7.1 mV; n = 8; N = 4; “ns”, no significant difference; p = 0.1; Student's two-tailed paired t test). Membrane potentials were corrected for liquid junction potential (10 mV).

In line with the absence of KCC2 expression in CSF-cNs demonstrated with in situ hybridization and immunostaining approaches, our functional analysis shows no KCC2 activity in CSF-cNs whereas KCC2 is a pivotal Cl^- extruder in mature DH GABA/glycine neurons.

Activation of $GABA_A$ receptors generates hyperpolarizations as well as depolarizations in spinal CSF-cNs

Cl^- transmembrane extrusion by KCC2 results in hyperpolarizing action of $GABA_A$-Rs activation in mature neurons. Therefore, one could suggest that the absence of KCC2 activity in CSF-cNs alongside with NKCC1 expression contribute to accumulate intracellular Cl^-, thus resulting in depolarizing action of $GABA_A$-Rs activation by Cl^- efflux through the receptor. To test this hypothesis, we investigated the effect of $GABA_A$-Rs activation on the membrane potential of CSF-cNs recorded in the cell-attached configuration, thus preserving intact intracellular Cl^- concentration. We used the reversal potential of K^+ channels (E_K) as a read out for CSF-cNs resting membrane potential as previously described in other cell types (Fricker et al., 1999; Verheugen et al., 1999). K^+ channels were activated with voltage-ramps from -140 to +200 mV ($-V_{pip}$) at 1 s intervals and CSF-cNs membrane potential estimated by measuring E_K at the intersection between the K^+ current and the fit to the linear component (Fig. 5Aa, red line). Among 23 CSF-cNs recorded, in the presence of DNQX (20 μM), strychnine (1 μM) and TTX (0.5 μM) pressure application of 1 mM GABA for 10 s induced a depolarization of 19 ± 8.9 mV in 16 cells (control membrane potential: -61.1 ± 10.8 mV; membrane potential during GABA application: -42 ± 9.0 mV, n = 16, N = 10; p = 3.7×10^{-7}, Student's two-tailed paired t-test; Fig. 5Ba, Bb, D and F). In the remaining 7 neurons, GABA induced a hyperpolarization of 9 ± 5.5 mV (control: -44.4 ± 10.3 mV; with GABA: -53.4 ± 10.2 mV; n = 7, N = 6; p = 0.0048, Student's two-tailed paired t-test; Fig. 5Ca, Cb, E and F). Note that the control membrane potentials between the two groups of CSF-cNs (-61.1 ± 10.8 mV and -44.4 ± 10.3 mV for cells responding with

depolarization and hyperpolarization, respectively) were significantly different (p = 0.0042, unpaired Student's t-test). Finally, bath application of $GABA_A$-Rs antagonists gabazine (10 µM) and picrotoxin (100 µM) blocked the GABA modulation of CSF-cNs membrane potential (p = 0.4, Student's two-tailed paired t-test; Fig. 5H), thus demonstrating the involvement of $GABA_A$-Rs activation in the GABA effect.

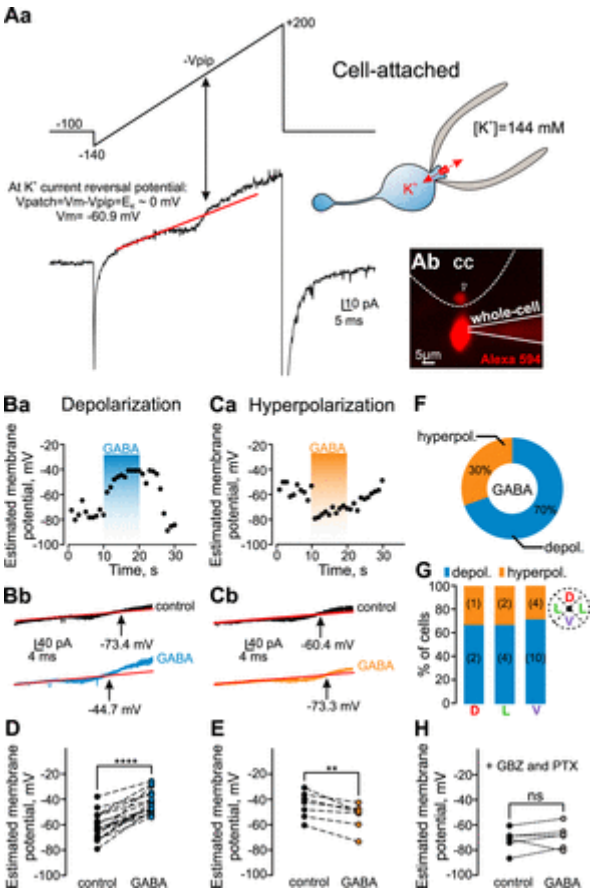

Figure 5.

The activation of $GABA_A$-Rs evokes both depolarizing and hyperpolarizing responses in spinal CSF-cNs. ***Aa***, The estimation of membrane potential in intact CSF-cNs was achieved by recording voltage-gated K^+ currents in the voltage-clamp tight-seal cell–attached configuration. Current (bottom trace) was evoked with a depolarizing ramp command from −140 mV ($-V_{pip}$) to +200 mV (top trace). The holding potential ($-V_{pip}$) was −100 mV with respect to the cell membrane potential. K^+ currents were recorded with a pipette solution containing 144 mM K^+ (see diagram). The K^+ currents reversal potential in cell-attached configuration was determined from the intersection of the linear fit (leak current, red line) and the K^+ current and used to measure the cell membrane potential. ***Ab***, CSF-cN typical morphology was confirmed after whole-cell dialysis with Alexa Fluor 594 and the visualization of the bud (open arrowhead in ***b***). The white dashed line delineates the CC. ***Ba***, The plot of the membrane potential versus the time recorded in one representative CSF-cN where GABA induces a depolarization of the membrane potential. ***Bb***, The 10 superimposed current traces before (black traces) and during GABA application (blue traces) showing that GABA evoked a depolarization. GABA was pressure-applied (1 mM, 10 s duration), and recording was performed in aCSF supplemented with DNQX (20 μM), strychnine (1 μM), and TTX (0.5 μM). Note the shift of K^+ current reversal (***Bb***) to the left in the presence of GABA (corresponding to a more depolarized membrane potential). ***C***, The time course of membrane potential (***a***) and 10 superimposed current traces (***b***) in control (black) and during GABA application (orange) from one CSF-cN where GABA induces a hyperpolarization of the membrane potential. CSF-cN membrane potential in both conditions was measured as shown in ***A***. ***D***,***E***, Line plots showing the membrane potential of individual CSF-cNs in control and during GABA application. GABA evoked in CSF-cNs a significant depolarization (panel ***D***; control, -61 ± 10.8 mV; GABA, -42 ± 9.0 mV; $n = 16$; $N = 10$; $^{****}p = 3.7 \times 10^{-7}$; Student's two-tailed paired *t* test) and hyperpolarization (panel ***E***; control, -44.4 ± 10.3 mV; GABA, -53.4 ± 10.2 mV; $n = 7$; $N = 6$; $^{**}p = 0.0048$; Student's two-tailed paired *t* test). ***F***, A pie graph indicating the proportion of CSF-cNs responding to GABA with a depolarization (blue; 70%; $n = 16$) or a hyperpolarization (orange; 30%; $n = 7$) of the estimated membrane potential. ***G***, A stacked bar graph showing the percentage of CSF-cNs showing depolarizing or hyperpolarizing responses to GABA along the dorsal–ventral axis of the CC. The region around the CC was subdivided in four quarters to determine the position of the recorded cell (inset, D, dorsal; L, lateral; V, ventral). The number of cells is indicated inside the bars. ***H***, The line plot of individual CSF-cNs showing that the variation in the membrane potential is mediated by the activation of $GABA_A$-Rs since GABA had no effect in the presence of the receptor antagonists GBZ (10 μM) and PTX (100 μM; control, -71.7 ± 8.6 mV; GABA, -69.3 ± 9.3 mV; $n = 6$; $N = 3$; "ns", no significant difference; $p = 0.4$; Student's two-tailed paired *t* test).

Altogether, these results revealed CSF-cNs as a heterogenous cell population in adult mice with different $GABA_A$-Rs modulation supporting different states of maturation, the immature CSF-cNs subgroup showing depolarizing GABA. Finally, as CSF-cNs with different maturation states were shown to have a different localization around the CC in postnatal rodents (Petracca et al., 2016), we analyzed the fraction of CSF-cNs that responded to GABA with either depolarization or hyperpolarization along the dorsal-ventral axis of the CC. However, as shown in Fig. 5G, there was no difference in the distribution of CSF-cNs with depolarizing or hyperpolarizing responses across dorsal, lateral, and ventral regions of the CC in adult mice (no statistical differences for all comparisons: dorsal versus ventral, dorsal versus lateral and ventral versus lateral; $p>0.99$, Fisher's exact test).

Depolarizing $GABA_A$ receptors generate AP in CSF-cNs

We next examined the effect of depolarizing GABA responses on CSF-cNs excitability. For each cell, we first determined the effect of GABA on the membrane potential (depolarization or hyperpolarization, Fig 6Aa and Ca or Ea, respectively) with cell-attached recording in tight-seal current-clamp configuration. Subsequently in the same cell, we analyzed in cell-attached voltage-clamp mode the GABA effects on CSF-cN action potential (AP) firing properties. (Perkins, 2006). In the presence of DNQX and strychnine, pressure application of GABA (1 mM for 5 s) induced a depolarization of 12.1 ± 4.9 mV (from -49.8 ± 6.1 mV to -37.7 ± 10.3 mV) and led to the generation of AP in 6 CSF-cNs out of 22 examined cells (N = 8) (27%; Fig. 6Aa, Ab, Ac, B and G). However, we also observed a reversible inhibition of the AP spontaneous activity in 6 CSF-cNs that responded to GABA with lower magnitude depolarizations (27%; 7.5 ±

5.1 mV; from -46.8 ± 3.0 to -39.3 ± 5.3 mV, n = 6; Fig. 6Ca, Cb, D and G). This shows that depolarizing GABA differentially modulates CSF-cNs in adult spinal cord by supporting AP generation or shunting inhibition. As expected, in CSF-cNs responding to GABA with hyperpolarizations (9.1 ± 4.9 mV; from -46 ± 4.8 mV to -55.1 ± 8.7 mV; n = 10; 45% of tested cells), the agonist induced a reversible inhibition of AP firing (Fig. 6Ea, Eb, F and G). Note that the resting membrane potentials measured in current-clamp cell-attached between cells responding with depolarization or hyperpolarization were similar ($p = 0.3$, unpaired Student's t-test) whereas we observed different values when resting potentials were estimated from K^+ current reversal potential (see above). This discrepancy may be explained by the fact that the measurement of the membrane potential with current-clamp cell-attached is inaccurate as the measured potential depends on seal resistance (Perkins, 2006). Finally, we checked that pressure applications of an external solution without GABA (aCSF) onto CSF-cNs did not evoke neither potential variations in current-clamp (n = 8, N = 2; Fig. 6H) nor AP discharge in voltage-clamp cell-attached recordings (n = 8, N = 2; Fig. 6I).

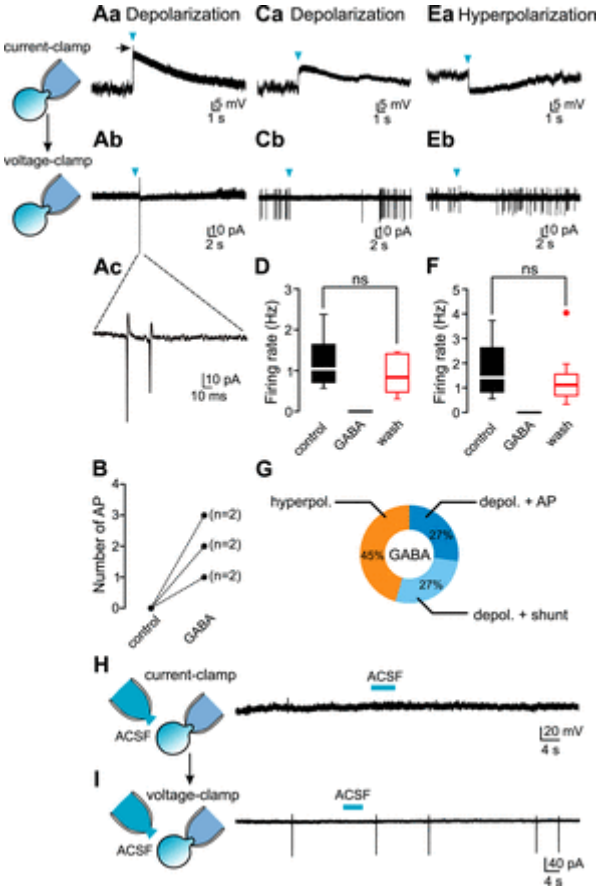
Aa Depolarization
Ca Depolarization
Ea Hyperpolarization
current-clamp
5 mV
1 s
Ab
Cb
Eb
voltage-clamp
10 pA
2 s
Ac
10 pA
10 ms
D
F
ns
Firing rate (Hz)
control
GABA
wash
B
Number of AP
(n=2)
G
hyperpol.
depol. + AP
depol. + shunt
45% GABA
27%
H
current-clamp
ACSF
20 mV
4 s
I
voltage-clamp
40 pA

Figure 6.

Depolarizing GABA triggers AP or mediates shunting inhibition in CSF-cNs. A, Pressure application of GABA (1 mM for 5 s, arrowheads) in the presence of DNQX (20 μM) and strychnine (1 μM) induced a depolarization (from −47.4 mV to −29.1 mV; the arrow indicates the presence of an AP) in one CSF-cN recorded in current-clamp cell–attached mode (a). In the same cell recorded in voltage-clamp cell–attached mode, GABA induced the discharge of AP currents (b,c). B, The number of AP evoked by GABA in CSF-cNs ("n" indicates the number of cells for each AP discharge patterns). C, CSF-cNs with GABA-mediated depolarization (a, current-clamp cell-attached; from −47.6 mV to −36.6 mV) and an inhibition of the AP spontaneous activity following GABA application (b, voltage-clamp cell–attached). D, A summary box-and-whisker plot showing that GABA abolished in a reversible manner the AP spontaneous activity of CSF-cNs that responded by depolarization (control, 1.2 ± 0.6 Hz; wash, 0.9 ± 0.5 Hz; n = 6; N = 5; "ns", no significant difference; p = 0.1; Student's two-tailed paired t test). E, Current-clamp (a) and voltage–clamp recordings (b) of a representative CSF-cN that responded to GABA by a hyperpolarization (a, from −44.7 mV to −54.2 mV) with a reduction of the firing frequency (b). F, A summary box-and-whisker plot of AP spontaneous activity of CSF-cNs responding by hyperpolarization in control, GABA, and after washing out the agonist (control, 1.7 ± 1.2 Hz; wash, 1.3 ± 1.1 Hz; n = 10; N = 5; "ns", no significant difference; p = 0.3; Wilcoxon matched-pair signed–rank test). G, A pie graph indicating the proportion of CSF-cNs that respond to GABA in current-clamp and voltage-clamp cell–attached recordings with depolarizations triggering AP discharge (dark blue; 27%; n = 6), depolarizations inducing a shunt inhibition of tonic AP activity (light blue; 27%; n = 6), and hyperpolarizations (orange; 45%; n = 10). H–I, Pressure applications of external solution without GABA (aCSF) did not evoke either potential variations in CSF-cNs recorded in current-clamp cell–attached (H) or AP discharge in voltage-clamp cell–attached recordings (I).

GABA evokes cytosolic Ca^{2+} elevations dependent on voltage-gated Ca^{2+} channels and NKCC1 transporters.

Previous studies have demonstrated that $GABA_A$-Rs promote depolarization-dependent elevations of intracellular calcium concentration ($[Ca^{2+}]_i$) in young neurons (Owens et al., 1996; Garaschuk et al., 2000; Reali et al., 2011). We thus investigated whether depolarizing $GABA_A$-Rs in spinal CSF-cNs of adult spinal cord induces changes in $[Ca^{2+}]_i$ using calcium imaging with the GCaMP6f sensor, selectively expressed in CSF-

cNs by Cre/lox recombination (PKD-CaMP6f mice, see Methods). $[Ca^{2+}]_i$ measurements were performed in the presence of DNQX (20 μM), strychnine (1 μM) and CGP54626 (10 μM) to selectively block glutamate AMPA/kainate, glycine and $GABA_B$ receptors, respectively. In line with our previous observations of distinct subpopulations of GABA-responding CSF-cNs, pressure application of GABA (1 mM, 10 s duration) induced an increase in $[Ca^{2+}]_i$ in 45 % of CSF-cNs (29 cells out of 65 CSF-cNs) whereas 55% of CSF-cNs did not respond to GABA by calcium rise (36 cells out of 65 CSF-cNs; Fig. 7A, C and E). In contrast, application of aCSF solution with high K^+ (20 mM, 10 s duration) induced $[Ca^{2+}]_i$ rise in most CSF-cNs (88%, 23 cells out of 26 CSF-cNs; p = 0.00013, Fisher's exact test; Fig. 7B, D and E). However, by comparing cells showing responses, we report that GABA and high-K^+ aCSF induced similar $[Ca^{2+}]_i$ rise (GABA: 79.5 ± 81.6 % $\Delta F/F_0$, n = 29, N = 8; high-K^+: 93.4 ± 90.2% $\Delta F/F_0$, n = 23, N = 2; p = 0.2, Mann Whitney-test; Fig. 7F). Next, we studied the impact of different treatments on GABA-mediated $[Ca^{2+}]_i$ changes. As we experienced rapid bleaching of the dye preventing repetitive $[Ca^{2+}]_i$ measurements in the same cell, we determined the proportions of CSF-cNs that respond to GABA by $[Ca^{2+}]_i$ rise under different experimental conditions and compared it to control (GABA alone). As shown in Fig. 7E, in the presence of aCSF solution lacking Ca^{2+} (0-Ca^{+2}) or containing the voltage-dependent calcium channel blocker cadmium (Cd^{+2}, 200 μM), the proportion of CSF-cNs showing $[Ca^{2+}]_i$ increase following GABA application was significantly lower (0-Ca^{+2}: 2/20, 10%, p = 0.007; Cd^{2+}: 7/44, 15%, p = 0.002; Fisher's exact test). Moreover, the inhibition of the intracellular Cl^- accumulator NKCC1 by the selective blocker bumetanide (BTN, 20 μM) significantly reduced the proportion of responding CSF-cNs compared to control (7/37, 19%; p = 0.010, Fisher's exact test, Fig. 7E).

Altogether, these results show that NKCC1 participate in accumulating intracellular Cl^- in CSF-cNs allowing depolarizing $GABA_A$ receptors-mediated calcium influx through voltage-gated calcium channels.

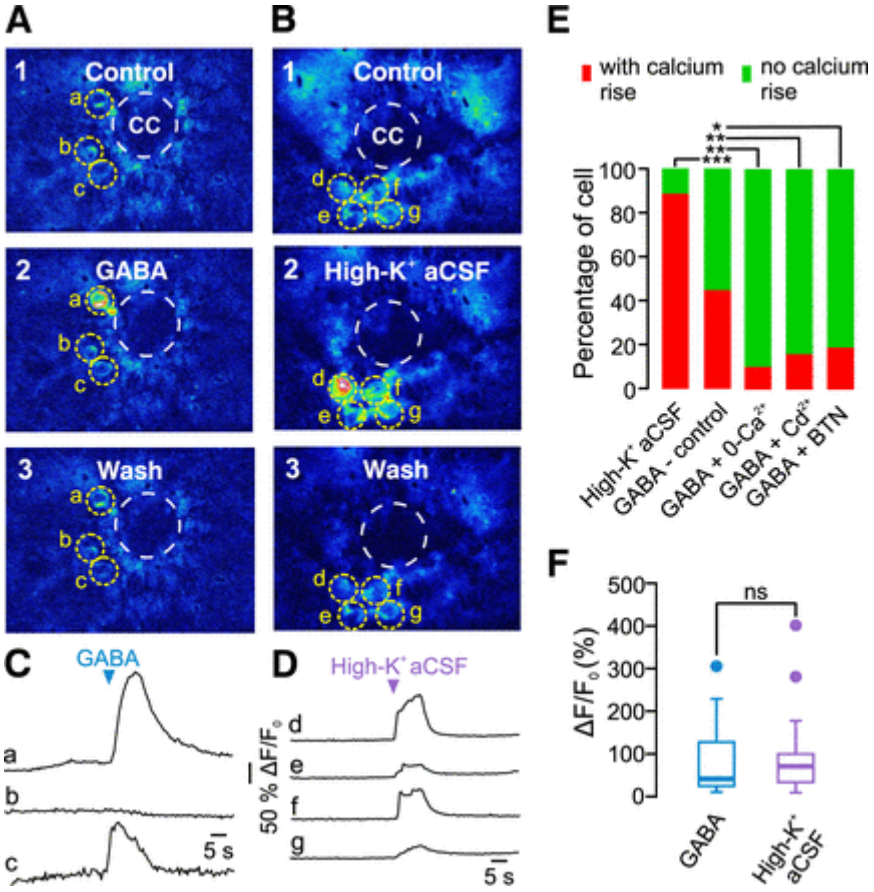

Figure 7.

The activation of $GABA_A$-Rs evokes calcium elevations in CSF-cNs. ***A***,***B***, Representative images illustrating the baseline fluorescence (1), the maximum fluorescence increase after pressure application of GABA (1 mM) or high-K^+ aCSF (20 mM, 2) for 10 s and after the recovery period (3, wash) in CSF-cNs expressing the calcium sensor GCaMP6f. GABA and high-K^+ aCSF were applied in the presence of DNQX (20 µM), strychnine (1 µM), and CGP54626 (10 µM). Images are presented in pseudocolor (black, low fluorescence; red, high fluorescence). Yellow dashed lines indicate the ROI drawn on CSF-cN soma. Dashed white lines delineate the CC. ***C***,***D***, Time course of the net fluorescence changes during application of GABA (***C***) and high-K^+ aCSF (***D***) from cells shown in ***A*** and ***B***, respectively. Note that GABA failed to induce a fluorescence rise in cell (b). ***E***, A stacked bar graph showing the percentage of CSF-cNs that responded by an increase in $[Ca^{2+}]_i$ upon pressure application of high-K^+ aCSF or GABA in control conditions or under perfusion with calcium-free aCSF (0-Ca^{2+}), aCSF supplemented with the voltage-gated Ca^{2+} channel blocker cadmium (Cd^{2+}, 200 µM), or BTN (20 µM), a selective inhibitor of NKCC1 transporter (***$p = 0.00013$; high-K^+ aCSF compared with control GABA; **$p = 0.007$; ** $p = 0.002$; *$p = 0.010$; GABA control compared, respectively, to 0-Ca^{2+}, Cd^{2+}, and BTN; Fisher's exact test). ***F***, A box-and-whisker plot for the normalized fluorescence variation ($\Delta F/F_0$) analyzed in CSF-cNs that responded to GABA and high-K^+ aCSF (GABA,

79.5 ± 81.6%; $n = 29$; $N = 8$; high-K^+ aCSF, 93.4 ± 90.2%; $n = 23$; $N = 2$; "ns", no significant difference; $p = 0.2$; Mann–Whitney test).

No hyperpolarizing modulation by $GABA_B$ receptors in spinal CSF-cNs

Medullo-spinal CSF-cNs in adult rodents were shown to express metabotropic G protein-coupled $GABA_B$-Rs (Margeta-Mitrovic et al., 1999; Jurčić et al., 2019). As hyperpolarizing signaling of $GABA_B$-Rs depends on the gating of inwardly rectifying K^+ (GIRK) channels, we tested whether activation of $GABA_B$-Rs generates outward K^+ currents in spinal CSF-cNs that exhibit depolarizing $GABA_A$-Rs responses. The experimental design consisted in recording CSF-cNs first in current-clamp cell-attached configuration to determine the effect of GABA on the membrane potential without perturbation of intracellular Cl^- and subsequently, we established a whole-cell configuration of the same cell and recorded in voltage-clamp mode at a holding potential of -50 mV, the effect of $GABA_B$-Rs activation on the holding current. We found that in CSF-cNs with depolarizing GABA responses recorded in cell-attached (Fig. 8Aa), bath application of the selective $GABA_B$-Rs agonist baclofen (100 μM) in the same cell had no effects on the holding current (Fig. 8Ab1; n = 6). Remarkably, these results indicate that CSF-cNs with depolarizing $GABA_A$-Rs also lack $GABA_B$Rs-dependent hyperpolarizing regulation.

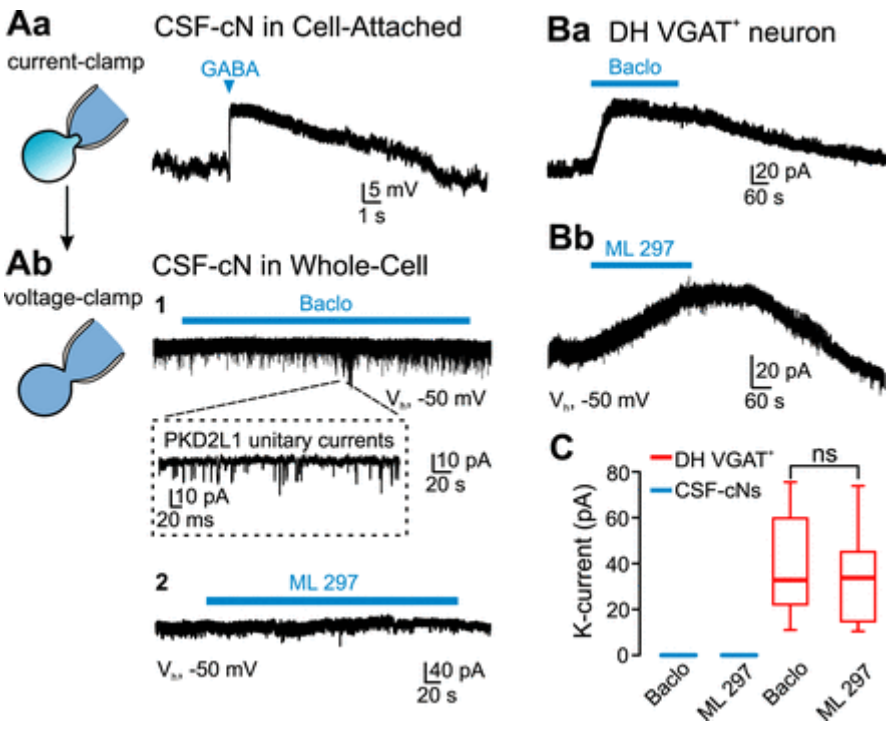

Figure 8.

Spinal CSF-cNs do not express $GABA_B$-R–mediated GIRK potassium currents. ***A***, One CSF-cN recorded in current-clamp cell–attached configuration (***a***) showing a depolarization of the membrane potential following pressure-applied GABA (1 mM, 5 s). In the same cell, voltage-clamped at −50 mV in whole-cell configuration, bath application of baclofen (100 µM), the selective $GABA_B$-R agonist, had no effect on the holding current (***b1***). Note the single-channel activity (inset) mediated by the PKD2L1 channel activity, as previously described in CSF-cNs. In the same CSF-cN recorded in voltage-clamp whole-cell configuration, bath application of ML297 (100 µM, ***b2***), the GIRK1/2 selective activator, did not generate K^+ currents at a holding potential of −50 mV. ***B***, In DH $VGAT^+$ neurons recorded with voltage-clamp whole-cell at a holding potential of −50 mV, both baclofen (***a***) and ML297 (***b***) induced an outward K^+ current. Baclofen and ML297 were bath applied at a concentration of 100 µM. ***C***, A summary box-and-whisker plot showing that baclofen and ML297 failed to induce current responses in CSF-cNs ($n = 6$ and $n = 11$, respectively; $N = 2$), while they evoke K^+ outward currents with similar amplitudes in DH $VGAT^+$ neurons (baclofen,

38.8 ± 22.2 pA; $n = 12$; $N = 3$; ML297, 34.8 ± 21.6 pA; $n = 7$; $N = 3$; "ns", no significant difference; $p = 0.7$; unpaired Student's *t* test).

We further investigated the mechanisms underlying the lack of $GABA_B$ receptors-dependent K^+ currents, assuming that GIRK channels are not expressed in spinal CSF-cNs. To test this hypothesis, we applied on spinal CSF-cNs ML297, a direct and selective activator of GIRK1/2 channels, the most abundant neuronal GIRK channels (Gonzalez et al., 2018; Kimura et al., 2020; Luo et al., 2022). However, ML297 failed to elicit an increase in the holding currents in CSF-cNs (Fig. 8Ab2 and C; n = 11, N = 2). In contrast and in agreement with previous reports (Kangrga et al., 1991; Kimura et al., 2020), bath application of baclofen (100 μM) or ML297 (100 μM) induced similar outward K^+ currents in DH $VGAT^+$ neurons with amplitudes of respectively 38.8 ± 22.2 pA (n = 12, N = 3) and 34.8 ± 21.2 pA (n = 7, N = 3 ; p = 0.7, unpaired Student's t-test) (Fig. 8Ba, Bb and C), which confirms the potent modulator effect of ML297 on GIRK channels. Therefore, the deficit in GIRK expression probably supports the lack of $GABA_B$-Rs-mediated hyperpolarization in spinal CSF-cNs.

Discussion

Immature neurons in adult mammalian central nervous system (CNS) represent a potential reservoir of young cells that may be mobilized under physiological or pathological conditions (La Rosa et al., 2019). Immature neurons were generally thought to localize in the subgranular zone of the hippocampal dentate gyrus and the subventricular zone of the lateral ventricles, but recent studies have suggested the presence of immature neurons on a large scale in other parts of the CNS as well, such as the spinal cord and the hindbrain (Rusanescu and Mao, 2014; Rusanescu, 2016).

Specifically, an intriguing expression of immature neuronal markers has been observed in some medullo-spinal CSF-cNs of adult rodents, which led to the hypothesis of the presence of two subpopulations of CSF-cNs with distinct maturity states (Kútna et al., 2014; Orts-Del'immagine et al., 2014; Petracca et al., 2016). However, whether these two subgroups of CSF-cNs have different GABAergic signaling was not yet known. In the present study, we demonstrate that GABA, acting via $GABA_A$-Rs, produces in spinal CSF-cN population either hyperpolarizations or depolarizations that trigger AP discharge or shunting of their tonic activity. In agreement with these results, we found that a proportion of CSF-cNs express the NKCC1 transporter but KCC2 expression was not detected, which allows intracellular Cl^- accumulation and depolarizing GABA in these cells. Our study further shows that GABA recruits voltage-gated calcium channels to increase $[Ca^{2+}]_i$ in CSF-cNs. Finally, we found that CSF-cNs don't express G protein-activated inwardly rectifying K^+ (GIRK) currents, resulting in the absence of $GABA_B$ receptor-mediated inhibition.

Immature GABA signaling in CSF-cNs of adult spinal cord

Previous studies with intracellular recording techniques have shown that CSF-cNs in adult mice receive GABAergic synaptic inputs that have been thought to mediate $GABA_A$ receptor-dependent inhibition (Orts-Del'immagine et al., 2012; Jurčić et al., 2019). By using cell-attached recordings for maintaining intact the intracellular milieu, we show instead that GABA generates depolarizations in 70% of the recorded CSF-cNs by acting on $GABA_A$-Rs. A similar observation was previously made in spinal CSF-cNs of postnatal rats and juvenile turtle (Marichal et al., 2009; Reali et al., 2011), though our data are the first showing recordings of depolarizations and spikes evoked by GABA in fully adult animals. Moreover, we found that a large fraction (45%) of CSF-cNs

responded to GABA by elevations of $[Ca^{2+}]_i$ dependent on the recruitment of voltage-gated Ca^{2+} channels. As described in a wide range of developing brain structures (Eilers et al., 2001; Ben-Ari, 2002; Ge et al., 2006), GABA may therefore couple with Ca^{2+} for driving maturation and integration of CSF-cNs into the spinal circuit.

Depolarizing GABA in CSF-cNs may imply a differential expression profile between the Cl^- extruder KCC2 and the Cl^- loader NKCC1 as described in immature neurons (Kilb, 2021). Indeed, *in situ* hybridization, immunohistofluorescence and functional analysis indicate a lack of KCC2 expression and a consistent low capacity of CSF-cNs for extruding Cl^- when imposing a constant Cl^- load through the recording pipette. In contrast, we observed in neurons of the spinal dorsal horn, considered as mature cells, an active Cl^- extrusion mediated by KCC2 transport under Cl^- load, as previously described (Cordero-Erausquin et al., 2005; Ferrini et al., 2020). However, we cannot exclude the expression of other types of isotonic K^+-Cl^- cotransporters in CSF-cNs that may participate in reducing the intracellular Cl^- concentration (Race et al., 1999; Lucas et al., 2012), thus allowing the switch between depolarizing GABA and hyperpolarization modulation in CSF-cNs.

In addition to the apparent low capacity of CSF-cNs to extrude Cl^-, we found that a proportion of CSF-cNs express the Cl^- accumulator NKCC1. Therefore, one could suggest that the depolarizing GABA responses recorded in CSF-cNs are the result of a differential expression of Cl^- transporters, NKCC1 being predominant over KCC2, thus allowing high intracellular Cl^- concentrations in CSF-cNs (Kilb, 2021). Consistent with this interpretation, blockade of NKCC1 with bumetanide reduced the proportion of CSF-cNs responding with intracellular calcium elevation evoked by GABA-dependent depolarizations. However, *in situ* hybridization showed a proportion of CSF-cNs

expressing NKCC1 (18.3%) lower than the fraction of CSF-cNs that responded by depolarizations (70%) or calcium elevations (45%) upon GABA application. This suggests that other types of transporters may be involved in intracellular accumulation of Cl^- in CSF-cNs as described in other young neurons (Gonzalez-Islas et al., 2009). This hypothesis is supported by the observation that GABA-dependent calcium rise was still measured in some CSF-cNs after application of the NKCC1 blocker bumetanide. Moreover, we cannot exclude an underestimation of the number of NKCC1-expressing CSF-cNs with *in situ* hybridization because of fluctuations in transcription (Kaern et al, 2005) or lack in detection as gene encoding NKCC1 is transcribed at low levels in neurons (Virtanen et al., 2020).

GABA inhibition in the CNS is also mediated by the activation of $GABA_B$-Rs**,** which recruits G-protein-activated inwardly rectifying K^+ (GIRK) channels and generates hyperpolarization (Pinard et al., 2010). However, we showed that baclofen, a selective $GABA_B$-R agonist, does not activate GIRK currents hence indicating the absence of $GABA_B$Rs-dependent hyperpolarizing modulation in CSF-cNs. $GABA_B$-Rs are expressed and functional early in development, though they are not yet involved in regulating neuronal excitability by gating GIRK channels in most developing brain regions (Gaiarsa and Porcher, 2013). Indeed, GIRK inhibition occurs in neurons after several weeks of postnatal maturation, GIRK channels being expressed and functionally coupled with $GABA_B$-Rs the latest between the third and the fifth postnatal week in the brain (Nurse and Lacaille, 1999; Lei and McBain, 2003). As we conducted our experiments with 7-10 weeks old mice, thus beyond the expected maturation period of GIRK channels, the absence of $GABA_B$ receptor-mediated GIRK inhibition further

supports the notion that CSF-cNs are under development or in an intermediate maturation state in adult mice.

Different GABAergic signaling may reflect CSF-cNs with distinct maturity states

In addition to a depolarizing effect of $GABA_A$-Rs, we observed GABA-mediated hyperpolarizations in CSF-cNs with cell-attached recordings, suggesting that CSF-cNs in the adult spinal cord are present around the CC in two putative distinct maturational states, immaturity with depolarizing $GABA_A$-Rs responses and a more mature state with hyperpolarizing modulation. This observation is supported by previous studies showing that subgroups of CSF-cNs have different expression levels of the neuronal nuclear protein (NeuN), a marker of neuronal differentiation and maturation (Orts-Del'immagine et al., 2014; Orts-Del'Immagine et al., 2017). Interestingly, CSF-cNs evolving in different states of maturity and with depolarizing and hyperpolarizing GABA transmission were observed as soon as the first days of postnatal life in rodents (Marichal et al., 2009; Petracca et al., 2016). Our data thus reinforced the idea that subpopulations of CSF-cNs with distinct developmental states are maintained until adulthood, the reserve of immature CSF-cNs being probably recruited then functionally incorporated into the local network in physiological or pathological conditions (La Rosa et al., 2019).

The presence of two subgroups of CSF-cNs is also supported by the observation that CSF-cNs with opposite GABA responses have different resting membrane potentials. Notably, by measuring the reversal potential of K^+ currents in voltage-clamp cell-attached, we estimated the resting membrane potential of CSF-cNs and showed that neurons with depolarizing GABA responses have a significantly more negative membrane potential compared to cells with hyperpolarizing GABA. Subpopulations of

neurons with different maturity states were shown to express distinct spike profiles, as well. Interestingly, CSF-cNs were shown to discharge action potentials in tonic or phasic mode (Orts-Del'immagine et al., 2012) and therefore, one could suggest experiments consisting in correlating the GABA polarity in CSF-cNs with their discharge patterns and spikes properties for further supporting the hypothesis of two CSF-cNs subgroups. The determination of different values of E_{GABA} in CSF-cNs could additionally support the idea of two subpopulations of CSF in adult mice. E_{GABA} can classically be accessed by using gramicidin-perforated patch recordings (Akaike, 1996) but it was not possible to accomplish such experiments in our preparation. The fact that we conducted our experiments with spinal cord slices from adult animals may have restricted the potential of gramicidin to form prototypical ion channels as this membrane-perforating agent was used mostly in neuronal preparations from postnatal or young animals. Alternatively, one could consider an indirect determination of E_{GABA} by measuring the intracellular concentration of Cl^- in CSF-cNs using Cl^- sensitive fluorescent indicators (Kovalchuk and Garaschuk, 2012).

In conclusion, our data present the first evidence that a subgroup of CSF-cNs in adult mice presents GABAergic signaling hallmarks that support their immaturity state. Our results are in line with previous assumptions suggesting that some CSF-cNs are immature neurons in adult mice as they express markers being involved in cell migration and neurite outgrowth such as PSA-NCAM and DCX (Stoeckel et al., 2003b; Orts-Del'immagine et al., 2014). On the other hand, CSF-cNs were shown to take part in advanced physiological functions as they cooperate with other spinal neurons for the regulation of motor activity and posture in mice (Gerstmann et al., 2022). This suggests that immature CSF-cNs terminate their development and integrate into existing spinal

circuits, though the underlying mechanisms and how GABA signaling may tune such functional maturation of CSF-cNs remain to be elucidated.

Authors contributions

J.T., N.W., and R.S designed research; P.R., N.J., L.M., S.I., J.R.F., S.S., N.W., and R.S. performed research and analyzed data; N.W. and R.S. wrote the manuscript with help of the other authors.

References

Akaike N (1996) Gramicidin perforated patch recording and intracellular chloride activity in excitable cells. Prog Biophys Mol Biol 65:251-264.

Barthó P, Payne JA, Freund TF, Acsády L (2004) Differential distribution of the KCl cotransporter KCC2 in thalamic relay and reticular nuclei. Eur J Neurosci 20:965–975.

Ben-Ari Y (2002) Excitatory actions of gaba during development: the nature of the nurture. Nat Rev Neurosci 3:728–739.

Ben-Ari Y, Khalilov I, Kahle KT, Cherubini E (2012) The GABA excitatory/inhibitory shift in brain maturation and neurological disorders. Neuroscientist 18:467–486.

Blaesse P, Airaksinen MS, Rivera C, Kaila K (2009) Cation-chloride cotransporters and neuronal function. Neuron 61:820–838.

Böhm UL, Prendergast A, Djenoune L, Nunes Figueiredo S, Gomez J, Stokes C, Kaiser S, Suster M, Kawakami K, Charpentier M, Concordet J-P, Rio J-P, Del Bene F, Wyart C (2016) CSF-contacting neurons regulate locomotion by relaying mechanical stimuli to spinal circuits. Nat Commun 7:10866.

Bormann J, Hamill OP, Sakmann B (1987) Mechanism of anion permeation through channels gated by glycine and gamma-aminobutyric acid in mouse cultured spinal neurons. J Physiol 385:243–286.

Cordero-Erausquin M, Coull JAM, Boudreau D, Rolland M, De Koninck Y (2005) Differential maturation of GABA action and anion reversal potential in spinal lamina I neurons: impact of chloride extrusion capacity. J Neurosci 25:9613–9623.

Djenoune L, Khabou H, Joubert F, Quan FB, Nunes Figueiredo S, Bodineau L, Del Bene F, Burcklé C, Tostivint H, Wyart C (2014) Investigation of spinal cerebrospinal fluid-contacting neurons expressing PKD2L1: evidence for a conserved system from fish to primates. Front Neuroanat 8:26.

Eilers J, Plant TD, Marandi N, Konnerth A (2001) GABA-mediated Ca2+ signaling in developing rat cerebellar Purkinje neurons. J Physiol 536:429–437.

Ferrini F, Perez-Sanchez J, Ferland S, Lorenzo L-E, Godin AG, Plasencia-Fernandez I, Cottet M, Castonguay A, Wang F, Salio C, Doyon N, Merighi A, De Koninck Y (2020) Differential chloride homeostasis in the spinal dorsal horn locally shapes

synaptic metaplasticity and modality-specific sensitization. Nat Commun 11:3935.

Fidelin K, Djenoune L, Stokes C, Prendergast A, Gomez J, Baradel A, Del Bene F, Wyart C (2015) State-Dependent Modulation of Locomotion by GABAergic Spinal Sensory Neurons. Curr Biol 25:3035–3047.

Fricker D, Verheugen JA, Miles R (1999) Cell-attached measurements of the firing threshold of rat hippocampal neurons. J Physiol (Lond) 517 (Pt 3):791–804.

Gaiarsa J-L, Porcher C (2013) Emerging neurotrophic role of GABAB receptors in neuronal circuit development. Front Cell Neurosci 7:206.

Garaschuk O, Linn J, Eilers J, Konnerth A (2000) Large-scale oscillatory calcium waves in the immature cortex. Nat Neurosci 3:452–459.

Ge S, Goh ELK, Sailor KA, Kitabatake Y, Ming G, Song H (2006) GABA regulates synaptic integration of newly generated neurons in the adult brain. Nature 439:589–593.

Gerstmann K, Jurčić N, Blasco E, Kunz S, de Almeida Sassi F, Wanaverbecq N, Zampieri N (2022) The role of intraspinal sensory neurons in the control of quadrupedal locomotion. Curr Biol 32:2442-2453.e4.

Gonzalez JC,Chub N, Wenner P (2009) NKCC1 and AE3 Appear to Accumulate Chloride in Embryonic Motoneurons. J Neurophysiol 101(2):507-518

Gonzalez JC, Epps SA, Markwardt SJ, Wadiche JI, Overstreet-Wadiche L (2018) Constitutive and Synaptic Activation of GIRK Channels Differentiates Mature and Newborn Dentate Granule Cells. J Neurosci 38:6513–6526.

Haam J, Popescu IR, Morton LA, Halmos KC, Teruyama R, Ueta Y, Tasker JG (2012) GABA is excitatory in adult vasopressinergic neuroendocrine cells. J Neurosci 32:572–582.

Hille B (1992) Ionic channels of excitable membranes. Sinauer Associates Inc., Sunderland, MA 1-20.

Jalalvand E, Robertson B, Wallén P, Grillner S (2016) Ciliated neurons lining the central canal sense both fluid movement and pH through ASIC3. Nat Commun 7:10002.

Jurčić N, Er-Raoui G, Airault C, Trouslard J, Wanaverbecq N, Seddik R (2019) GABAB receptors modulate Ca2+ but not G protein-gated inwardly rectifying K+ channels in cerebrospinal-fluid contacting neurons of mouse brainstem. J Physiol (Lond) 597:631–651.

Jurčić N, Michelle C, Trouslard J, Wanaverbecq N, Kastner A (2021) Evidence for PKD2L1-positive neurons distant from the central canal in the ventromedial spinal cord and medulla of the adult mouse. Eur J Neurosci 54:4781–4803.

Kaern M, Elston TC, Blake WJ, Collins JJ (2005) **S**tochasticity in gene expression: from theories to phenotypes. Nat rev Genet 6:451-464

Kaila K (1994) Ionic basis of GABAA receptor channel function in the nervous system. Prog Neurobiol 42:489–537.

Kaila K, Voipio J, Paalasmaa P, Pasternack M, Deisz RA (1993) The role of bicarbonate in GABAA receptor-mediated IPSPs of rat neocortical neurons. J Physiol 464:273–289.

Kangrga I, Jiang MC, Randić M (1991) Actions of (-)-baclofen on rat dorsal horn neurons. Brain Res 562:265–275.

Kaufmann K, Romaine I, Days E, Pascual C, Malik A, Yang L, Zou B, Du Y, Sliwoski G, Morrison RD, Denton J, Niswender CM, Daniels JS, Sulikowski GA, Xie XS, Lindsley CW, Weaver CD (2013) ML297 (VU0456810), the first potent and selective activator of the GIRK potassium channel, displays antiepileptic properties in mice. ACS Chem Neurosci 4:1278–1286.

Kilb W (2021) When Are Depolarizing GABAergic Responses Excitatory? Front Mol Neurosci 14:747835.

Kimura M, Shiokawa H, Karashima Y, Sumie M, Hoka S, Yamaura K (2020) Antinociceptive effect of selective G protein-gated inwardly rectifying K+ channel agonist ML297 in the rat spinal cord. PLoS One 15:e0239094.

Knafo S, Fidelin K, Prendergast A, Tseng P-EB, Parrin A, Dickey C, Böhm UL, Figueiredo SN, Thouvenin O, Pascal-Moussellard H, Wyart C (2017) Mechanosensory neurons control the timing of spinal microcircuit selection during locomotion. Elife 6.

Kovalchuk Y, Garaschuk O (2012) Two-photon chloride imaging using MQAE in vitro and in vivo. Cold Spring Harb Protoc 2012:778-785.

Kurki SN, Uvarov P, Pospelov AS, Trontti K, Hübner AK, Srinivasan R, Watanabe M, Hovatta I, Hübner CA, Kaila K, Virtanen MA (2023) Expression patterns of NKCC1 in neurons and non-neuronal cells during cortico-hippocampal development. Cereb Cortex 33:5906-5923.

Kútna V, Ševc J, Gombalová Z, Matiašová A, Daxnerová Z (2014) Enigmatic cerebrospinal fluid-contacting neurons arise even after the termination of neurogenesis in the rat spinal cord during embryonic development and retain

their immature-like characteristics until adulthood. Acta Histochem 116:278–285.

La Rosa C, Ghibaudi M, Bonfanti L (2019) Newly Generated and Non-Newly Generated “Immature” Neurons in the Mammalian Brain: A Possible Reservoir of Young Cells to Prevent Brain Aging and Disease? J Clin Med 8:685.

Lei S, McBain CJ (2003) GABA B receptor modulation of excitatory and inhibitory synaptic transmission onto rat CA3 hippocampal interneurons. J Physiol (Lond) 546:439–453.

Lucas O, Hilaire C, Delpire E, Scamps F (2012) KCC3-dependent chloride extrusion in adult sensory neurons. Mol Cell Neurosci 50:211–220.

Luo H, Marron Fernandez de Velasco E, Wickman K (2022) Neuronal G protein-gated K+ channels. Am J Physiol Cell Physiol.

Madisen L et al. (2015) Transgenic mice for intersectional targeting of neural sensors and effectors with high specificity and performance. Neuron 85:942–958.

Margeta-Mitrovic M, Mitrovic I, Riley RC, Jan LY, Basbaum AI (1999) Immunohistochemical localization of GABA(B) receptors in the rat central nervous system. J Comp Neurol 405:299–321.

Marichal N, García G, Radmilovich M, Trujillo-Cenóz O, Russo RE (2009) Enigmatic central canal contacting cells: immature neurons in “standby mode”? J Neurosci 29:10010–10024.

Nurse S, Lacaille JC (1999) Late maturation of GABA(B) synaptic transmission in area CA1 of the rat hippocampus. Neuropharmacology 38:1733–1742.

Orts-Del’immagine A, Kastner A, Tillement V, Tardivel C, Trouslard J, Wanaverbecq N (2014) Morphology, Distribution and Phenotype of Polycystin Kidney

Disease 2-like 1-Positive Cerebrospinal Fluid Contacting Neurons in The Brainstem of Adult Mice. PLoS ONE 9:e87748.

Orts-Del'Immagine A, Seddik R, Tell F, Airault C, Er-Raoui G, Najimi M, Trouslard J, Wanaverbecq N (2016) A single polycystic kidney disease 2-like 1 channel opening acts as a spike generator in cerebrospinal fluid-contacting neurons of adult mouse brainstem. Neuropharmacology 101:549–565.

Orts-Del'Immagine A, Trouslard J, Airault C, Hugnot J-P, Cordier B, Doan T, Kastner A, Wanaverbecq N (2017) Postnatal maturation of mouse medullo-spinal cerebrospinal fluid-contacting neurons. Neuroscience 343:39–54.

Orts-Del'immagine A, Wanaverbecq N, Tardivel C, Tillement V, Dallaporta M, Trouslard J (2012) Properties of subependymal cerebrospinal fluid contacting neurons in the dorsal vagal complex of the mouse brainstem. J Physiol (Lond) 590:3719–3741.

Owens DF, Boyce LH, Davis MB, Kriegstein AR (1996) Excitatory GABA responses in embryonic and neonatal cortical slices demonstrated by gramicidin perforated-patch recordings and calcium imaging. J Neurosci 16:6414–6423.

Owens DF, Kriegstein AR (2002) Is there more to GABA than synaptic inhibition? Nat Rev Neurosci 3:715–727.

Payne JA, Rivera C, Voipio J, Kaila K (2003) Cation-chloride co-transporters in neuronal communication, development and trauma. Trends Neurosci 26:199–206.

Perkins KL (2006) Cell-attached voltage-clamp and current-clamp recording and stimulation techniques in brain slices. J Neurosci Methods 154:1–18.

Petracca YL, Sartoretti MM, Di Bella DJ, Marin-Burgin A, Carcagno AL, Schinder AF, Lanuza GM (2016) The late and dual origin of cerebrospinal fluid-contacting neurons in the mouse spinal cord. Development.

Pinard A, Seddik R, Bettler B (2010) GABAB receptors: physiological functions and mechanisms of diversity. Adv Pharmacol 58:231–255.

Race JE, Makhlouf FN, Logue PJ, Wilson FH, Dunham PB, Holtzman EJ (1999) Molecular cloning and functional characterization of KCC3, a new K-Cl cotransporter. Am J Physiol 277:C1210-1219.

Reali C, Fernández A, Radmilovich M, Trujillo-Cenóz O, Russo RE (2011) GABAergic signaling in a neurogenic niche of the turtle spinal cord. J Physiol (Lond) 589:5633–5647.

Rivera C, Voipio J, Payne JA, Ruusuvuori E, Lahtinen H, Lamsa K, Pirvola U, Saarma M, Kaila K (1999) The K+/Cl- co-transporter KCC2 renders GABA hyperpolarizing during neuronal maturation. Nature 397:251–255.

Rusanescu G (2016) Adult spinal cord neurogenesis: A regulator of nociception. Neurogenesis (Austin) 3:e1256853.

Rusanescu G, Mao J (2014) Notch3 is necessary for neuronal differentiation and maturation in the adult spinal cord. J Cell Mol Med 18:2103–2116.

Schmidt T, Ghaffarian N, Philippot C, Seifert G, Steinhäuser C, Pape H-C, Blaesse P (2018) Differential regulation of chloride homeostasis and GABAergic transmission in the thalamus. Sci Rep 8:13929.

Shechter R, Ziv Y, Schwartz M (2007) New GABAergic interneurons supported by myelin-specific T cells are formed in intact adult spinal cord. Stem Cells 25:2277–2282.

Sternberg JR, Prendergast AE, Brosse L, Cantaut-Belarif Y, Thouvenin O, Orts-Del'Immagine A, Castillo L, Djenoune L, Kurisu S, McDearmid JR, Bardet P-L, Boccara C, Okamoto H, Delmas P, Wyart C (2018) Pkd2l1 is required for mechanoception in cerebrospinal fluid-contacting neurons and maintenance of spine curvature. Nat Commun 9:3804.

Stoeckel M-E, Uhl-Bronner S, Hugel S, Veinante P, Klein M-J, Mutterer J, Freund-Mercier M-J, Schlichter R (2003a) Cerebrospinal fluid-contacting neurons in the rat spinal cord, a gamma-aminobutyric acidergic system expressing the P2X2 subunit of purinergic receptors, PSA-NCAM, and GAP-43 immunoreactivities: light and electron microscopic study. J Comp Neurol 457:159–174.

Stoeckel M-E, Uhl-Bronner S, Hugel S, Veinante P, Klein M-J, Mutterer J, Freund-Mercier M-J, Schlichter R (2003b) Cerebrospinal fluid-contacting neurons in the rat spinal cord, a gamma-aminobutyric acidergic system expressing the P2X2 subunit of purinergic receptors, PSA-NCAM, and GAP-43 immunoreactivities: light and electron microscopic study. J Comp Neurol 457:159–174.

Sun Y-G, Wu C-S, Renger JJ, Uebele VN, Lu H-C, Beierlein M (2012) GABAergic synaptic transmission triggers action potentials in thalamic reticular nucleus neurons. J Neurosci 32:7782–7790.

Tang D, Qian A-H, Song D-D, Ben Q-W, Yao W-Y, Sun J, Li W-G, Xu T-L, Yuan Y-Z (2015) Role of the potassium chloride cotransporter isoform 2-mediated spinal chloride homeostasis in a rat model of visceral hypersensitivity. Am J Physiol Gastrointest Liver Physiol 308:G767-778.

Verheugen JA, Fricker D, Miles R (1999) Noninvasive measurements of the membrane potential and GABAergic action in hippocampal interneurons. J Neurosci 19:2546–2555.

Vígh B, Manzano e Silva MJ, Frank CL, Vincze C, Czirok SJ, Szabó A, Lukáts A, Szél A (2004) The system of cerebrospinal fluid-contacting neurons. Its supposed role in the nonsynaptic signal transmission of the brain. Histol Histopathol 19:607–628.

Virtanen MA, Uranov P, Hübner CA, Kaila K (2020) NKCC1, an Elusive Molecular Target in Brain Development: Making Sense of the Existing Data. Cells 9:2607.

Yassin L, Radtke-Schuller S, Asraf H, Grothe B, Hershfinkel M, Forsythe ID, Kopp-Scheinpflug C (2014) Nitric oxyde signaling modulates synaptic inhibition in the superior paraolivary nucleus (SPN) via cGMP-dependent suppression of KCC2. Front Neural circuits 8:65.

Wang Y, Kakizaki T, Sakagami H, Saito K, Ebihara S, Kato M, Hirabayashi M, Saito Y, Furuya N, Yanagawa Y (2009) Fluorescent labeling of both GABAergic and glycinergic neurons in vesicular GABA transporter (VGAT)-venus transgenic mouse. Neuroscience 164:1031–1043.

Figure legends

Figure 1. CSF-cNs of adult spinal cord express NKCC1 but not KCC2 mRNAs. **A-C,** Confocal images showing in CSF-cNs the expression of NKCC1 mRNAs (arrows, green panel B) following fluorescence in situ hybridization (RNAScope). CSF-cNs were identified by the presence of PKD2L1 mRNA transcripts (red, panel A; merged image in panel C). **D-F,** In situ hybridization showed no expression of KCC2 (green, panel E) in PKD2L1^{+} CSF-cNs (red, panel D; merged image in panel F). However, we found a strong KCC2 mRNA signal in neurons negative for PKD2L1 and surrounding

the CC (arrowheads, panel E; merged image in panel F). Cell nuclei were counterstained with DAPI (blue, panel C and F). White dashed lines delineate the central canal. **G,** box-and-whisker plot showing the percentage of NKCC1 and KCC2 co-expression in $PKD2L1^+$ CSF-cNs (NKCC1, 20 cells out of 98 $PKD2L1^+$ cells; KCC2, 0 cells out of 87 $PKD2L1^+$ cells). **H,** Hippocampal CA1 region shows a strong KCC2 **(a)** but sparse NKCC1 mRNA signal **(b**, arrowhead**)** thus confirming the specificity of in situ hybridization experiments. **I,** The absence of KCC2 expression **(a)** together with the strong NKCC1 mRNA signal **(b)** in choroid plexus epithelial cells provide additional controls for the RNAScope procedure.

Figure 2. Absence of immunostaining for KCC2 in spinal CSF-cNs. **A-D,** confocal microscopy images showing no detectable KCC2 immunostaining (green, panels Ba and Bb) in adult CSF-cNs identified by their selective tdTomato expression (red, arrows in panels Aa and Ab; merged images in panels Da and Db). Panels Ab-Db show higher magnification of the boxed regions indicated in panels Aa-Da. However, neurons lacking tdTomato expression (non-CSF-cNs) show plasmalemmal immunostaining for KCC2 (arrowheads, panels Ba, Bb, Da and Db). Cell nuclei were counterstained with DAPI (blue, panels Ca and Cb; merged images in panels Da and Db). Panels Ab-Db are images at higher magnification from panels Aa-Da (white box). The central canal is delineated by white dashed lines. **E-L,** Expanded view of the $tdTomato^+$ CSF-cNs (red, E-H) and non-CSF-contacting $tdTomato^-$ neurons (I-L) highlighted in insets 1 and 2 of the merged picture in Db. Plasma membrane immunostaining for KCC2 (green) is detected in non-CSF-contacting neurons (panels I and J; merged image in panel L) but not in CSF-cNs (panels E and F; merged image in panel H). Nuclei were counterstained with DAPI (blue, panels G and K; merged images in panels H and L). **M-N,** Fluorescent

intensity line profile analysis for tdTomato (red), KCC2 (green) and DAPI (blue) of cells illustrated in insets 1 and 2. No KCC2 fluorescence is detected in the $tdTomato^+$ CSF-cN (M) whereas the fluorescence profile of KCC2 in the non-CSF-contacting $tdTomato^-$ neuron (N) indicates plasma membrane expression of KCC2. Intensity values for KCC2 and the tdTomato were normalized to the maximal value obtained from the non-CSF-contacting neuron and CSF-cN, respectively. **O-P,** Confocal image (O) and fluorescence intensity line profile analysis (P) showing KCC2 immunoreactivity in a dorsal horn neuron. The start points (0 μm) for the line profiles on the graphs in panels M, N and P, are illustrated by the orange dots of the line drawn on images H, L and O.

Figure 3. Adult spinal cord CSF-cNs have low Cl^- extrusion capacity. **A,** Cl^- extrusion measurements were performed in whole-cell configuration by recording $GABA_A$ receptors-mediated currents in cells maintained at different holding potentials (V_h: from -60 mV to +20 mV; steps of +20 mV) and with a pipette solution containing high Cl^- (29 mM). **B,** confocal image showing $VGAT^+$ (GABA/glycine) neurons in the spinal dorsal horn (white dash line) expressing the Venus fluorescent protein. **C-D,** representative averaged current traces evoked by GABA pressure applications (1 mM, 30 ms duration, arrowheads) recorded in one dorsal horn (DH) $VGAT^+$ neuron (C, red traces) and one CSF-cN (D, blue traces) in the presence of DNQX (20 μM) and strychnine (1 μM). **E,** mean GABA I-V curves recorded from DH $VGAT^+$ neurons (red) and CSF-cNs (blue). In CSF-cNs E_{GABA} (-33.1 mV, $R^2 = 0.8$; defined by the x-intercept of the linear fit, dashed line) is shifted to more positive values compared to DH VGAT+ neurons (-45.9 mV, $R^2 = 0.5$). Membrane potentials were corrected for liquid junction potential (10 mV). **F,** box-and-whisker plot for E_{GABA} measured in CSF-cNs (-30.5 ± 3.4 mV, n = 18, N = 4) and DH $VGAT^+$ neurons (-47.8 ± 13 mV, n = 19, N = 4). E_{GABA}

in CSF-cNs was significantly more depolarized compared to DH neurons (****p = 1.6 x 10^{-5}, unpaired Student's t-test). The grey dashed line shows the theoretical E_{GABA} (-38 mV) calculated with GHK equation. **G**, representative traces showing $GABA_A$-Rs currents evoked by pressure applications of GABA (arrowheads, 1 mM for 30 ms) in one representative CSF-cN maintained at different holding potentials in control (a) and in the presence of the $GABA_A$ receptor antagonists (b), gabazine (GBZ, 10 μM) and picrotoxin (PTX, 100 μM). **H,** box-and-whisker plot of GABA currents amplitude recorded at -60 mV showing that currents are fully abolished in the presence of GBZ and PTX (control: -231.3 ± 126.5 pA, n = 10, N=3). **I,** Pressure application of external solution without GABA (aCSF) did not change the holding current in CSF-cNs held at -60 mV.

Figure 4. Selective KCC2 inhibition shifts the E_{GABA} in DH $VGAT^+$ neurons but not in CSF-cNs. Representative current traces **(A, D)** and mean I-V plots **(B, E)** for GABA-induced currents recorded in DH $VGAT^+$ neurons (**A, B)** and CSF-cNs (**D, E**) in control (red and blue traces and circles for DH $VGAT^+$ and CSF-cNs, respectively) and in the presence of VU0463271 (VU, 10 μM; purple traces and circles), a KCC2 specific inhibitor. Currents were elicited with GABA pressure application (1 mM for 30 ms; arrowheads in A and D) in the presence of DNQX (20 μM), strychnine (1μM) and bumetanide (20 μM). In DH $VGAT^+$ neurons E_{GABA} obtained in the presence of VU0463271 is shifted to more positive values compared to control (B, control: E_{GABA} = -39.4 mV, R^2 = 0.9; VU: E_{GABA} = -28,9 mV, R^2 = 0.9; x-intercept of the linear fit) while it remained unchanged in CSF-cNs (E, control: E_{GABA} = -30.6 mV, R^2 = 0.9; VU: E_{GABA} = -28,6 mV, R^2 = 0.9). The grey dashed lines in B and E indicate E_{GABA} measured in control and in the presence of VU. **C and F,** summary box-and-whisker plots of E_{GABA}

from DH $VGAT^+$ neurons (red) and CSF-cNs (blue) in control and in the presence of VU0463271 (purple) conditions (DH $VGAT^+$ neurons, control: -41.5 ± 8,3 mV; VU: -31,6 ± 6.5 mV, n = 5, N = 4; **p = 0.0014, Student's two-tailed paired t-test and in CSF-cNs, control: -30.8 ± 2.9 mV; VU: -27.6 ± 7.1 mV, n = 8, N = 4; "ns", no significant difference, p = 0.1, Student's two-tailed paired t-test). Membrane potentials were corrected for liquid junction potential (10 mV).

Figure 5. Activation of $GABA_A$ receptors evokes both depolarizing and hyperpolarizing responses in spinal CSF-cNs. **Aa,** estimation of membrane potential in intact CSF-cNs was achieved by recording voltage-gated K^+ currents in the voltage-clamp tight-seal cell-attached configuration. Current (bottom trace) was evoked with a depolarizing ramp command from -140 mV ($-V_{pip}$) to +200 mV (top trace)**.** The holding potential ($-V_{pip}$) was -100 mV with respect to the cell membrane potential. K^+ currents were recorded with a pipette solution containing 144 mM K^+ (see cartoon). The K^+ currents reversal potential in cell-attached configuration was determined from the intersection of the linear fit (leak current, red line) and the K^+ current and used to measure the cell membrane potential. **Ab,** CSF-cN typical morphology was confirmed after whole-cell dialysis with Alexa 594 and the visualization of the bud (open arrowhead in b). The white dashed line delineates the central canal (CC). **Ba,** plot of the membrane potential versus time recorded in one representative CSF-cN where GABA induces a depolarization of the membrane potential. **Bb,** 10 superimposed current traces before (black traces) and during GABA application (blue traces) showing that GABA evoked a depolarization. GABA was pressure applied (1mM, 10 s duration) and recording was performed in aCSF supplemented with DNQX (20 μM), strychnine (1 μM) and TTX (0.5 μM). Note the shift of K^+ current reversal (Bb) to the left in the

presence of GABA (corresponding to a more depolarized membrane potential). **C,** time course of membrane potential (a) and 10 superimposed current traces (b) in control (black) and during GABA application (orange) from one CSF-cN where GABA induces a hyperpolarization of the membrane potential. CSF-cN membrane potential in both conditions was measured as shown in (A). **D and E,** Line plots showing the membrane potential of individual CSF-cNs in control and during GABA application. GABA evoked in CSF-cNs a significant depolarization (panel D; control: -61 ± 10.8 mV; GABA: -42 ± 9.0 mV, n = 16, N = 10; ****p = 3.7 x 10^{-7}, Student's two-tailed paired t-test) and hyperpolarization (panel E; control: -44.4 ± 10.3 mV; GABA: -53.4 ± 10.2 mV, n = 7, N = 6; **p = 0.0048, Student's two-tailed paired t-test). **F,** pie graph indicating the proportion of CSF-cNs responding to GABA with a depolarization (blue; 70%, n = 16) or a hyperpolarization (orange; 30%, n = 7) of the estimated membrane potential. **G,** stacked bar-graph showing the percentage of CSF-cNs showing depolarizing or hyperpolarizing responses to GABA along the dorsal-ventral axis of the CC. The region around the CC was subdivided in 4 quarters to determine the position of the recorded cell (inset, D: dorsal; L: lateral; V: ventral). The number of cells is indicated inside the bars. **H,** line plot of individual CSF-cNs showing that the variation in the membrane potential is mediated by activation of $GABA_A$ receptors since GABA had no effect in the presence of the receptor antagonists gabazine (GBZ, 10 μM) and picrotoxin (PTX, 100 μM) (control: -71.7 mV ± 8.6 mV; GABA: -69.3 ± 9.3 mV, n = 6, N = 3; "ns", no significant difference, p = 0.4, Student's two-tailed paired t-test).

Figure 6. Depolarizing GABA triggers AP or mediates shunting inhibition in CSF-cNs. **A,** pressure application of GABA (1 mM for 5 s, arrowheads) in the presence of DNQX (20 μM) and strychnine (1 μM) induced a depolarization (from -47.4 mV to -29.1 mV;

the arrow indicates the presence of an action potential) in one CSF-cN recorded in current-clamp cell-attached mode (a). In the same cell recorded in voltage-clamp cell-attached mode, GABA induced the discharge of action potential (AP) currents (b and c). **B,** Number of AP evoked by GABA in CSF-cNs ("n" indicates the number of cells for each AP discharge patterns). **C,** CSF-cNs with GABA-mediated depolarization (a, current-clamp cell-attached; from -47.6 mV to -36.6 mV) and an inhibition of the AP spontaneous activity following GABA application (b, voltage-clamp cell-attached). **D,** summary box-and-whisker plot showing that GABA abolished in a reversible manner the AP spontaneous activity of CSF-cNs that responded by depolarization (control: 1.2 ± 0.6 Hz; wash: 0.9 ± 0.5 Hz, n = 6, N= 5; "ns", no significant difference, p = 0.1, Student's two-tailed paired t-test). **E,** current-clamp (a) and voltage-clamp recordings (b) of a representative CSF-cN that responded to GABA by a hyperpolarization **(**a, from -44.7 mV to -54.2 mV) with a reduction of the firing frequency (b). **F,** summary box-and-whisker plot of AP spontaneous activity of CSF-cNs responding by hyperpolarization in control, GABA and after washing out the agonist (control: 1.7 ± 1.2 Hz; wash: 1.3 ± 1.1 Hz, n = 10, N = 5; "ns", no significant difference, p = 0.3, Wilcoxon matched-pairs signed rank test). **G,** pie graph indicating the proportion of CSF-cNs that respond to GABA in current-clamp and voltage-clamp cell-attached recordings with depolarizations triggering AP discharge (dark blue; 27%, n = 6), depolarizations inducing a shunt inhibition of tonic AP activity (light blue; 27%, n=6) and hyperpolarizations (orange; 45%, n=10). **H-I,** pressure applications of external solution without GABA (aCSF) did not evoke either potential variations in CSF-cNs recorded in current-clamp cell-attached (H) or AP discharge in voltage-clamp cell-attached recordings (I).

Figure 7. Activation of $GABA_A$ receptors evokes calcium elevations in CSF-cNs. **A and B,** representative images illustrating the baseline fluorescence (1), the maximum fluorescence increase after pressure application of GABA (1mM) or high-K^+ aCSF (20 mM, 2) for 10 s and after the recovery period (3, wash) in CSF-cNs expressing the calcium sensor GCaMP6f. GABA and high-K^+ aCSF were applied in the presence of DNQX (20 μM), strychnine (1 μM) and CGP54626 (10 μM). Images are presented in pseudocolour (black: low fluorescence; red: high fluorescence). Yellow dashed lines indicate the regions of interest (ROI) drawn on CSF-cNs soma. Dashed white lines delineate the central canal (CC). **C and D,** time course of the net fluorescence changes during application of GABA (C) and high-K^+ aCSF (D) from cells shown in **(A)** and **(B)**, respectively. Note that GABA failed to induce a fluorescence rise in cell (b). **E,** stacked bar-graph showing the percentage of CSF-cNs that responded by an increase in $[Ca^{2+}]_i$ upon pressure application of high-K^+ aCSF or GABA in control conditions or under perfusion with calcium-free aCSF (0-Ca^{2+}), aCSF supplemented with the voltage-gated Ca^{2+} channel blocker cadmium ($Cd^{2+,}$ 200 μM) or bumetanide (BTN, 20 μM), a selective inhibitor of NKCC1 transporter (***p = 0.00013, high-K^+ aCSF compared to control GABA; **p = 0.007, ** p = 0.002, *p = 0.010, GABA control compared respectively to 0-Ca^{2+}, Cd^{2+} and BTN, Fisher's exact test). **F,** box-and-whisker plot for the normalized fluorescence variation ($\Delta F/F_0$) analyzed in CSF-cNs that responded to GABA and high-K^+ aCSF (GABA: 79.5 ± 81.6 %, n = 29, N = 8; high-K^+ aCSF: 93.4 ± 90.2%, n = 23, N = 2; "ns", no significant difference, p = 0.2, Mann Whitney-test).

Figure 8. Spinal CSF-cNs do not express $GABA_B$ receptors-mediated GIRK potassium currents. **A,** One CSF-cN recorded in current-clamp cell-attached configuration (a) showing a depolarization of the membrane potential following pressure-applied GABA

(1mM, 5 s). In the same cell, voltage-clamped at -50 mV in whole-cell configuration, bath application of baclofen (100 μM), the selective $GABA_B$ receptors agonist, had no effect on the holding current (b1). Note the single-channel activity (inset) mediated by the PKD2L1 channel activity, as previously described in CSF-cNs. In the same CSF-cN recorded in voltage-clamp whole cell configuration, bath application of ML297 (100 μM, b2), the GIRK1/2 selective activator, did not generate K^+ currents at a holding potential of -50 mV. **B,** in DH $VGAT^+$ neurons recorded with voltage-clamp whole-cell at a holding potential of -50 mV, both baclofen (a) and ML297 (b) induced an outward K^+ current. Baclofen and ML297 were bath applied at a concentration of 100 μM. **C,** summary box-and-whisker plot showing that baclofen- and ML297 failed to induce current responses in CSF-cNs (n = 6 and n = 11, respectively, N = 2) while they evoke K^+ outward currents with similar amplitudes in DH $VGAT^+$ neurons (baclofen: 38.8 ± 22.2 pA, n = 12, N = 3 ; ML297: 34.8 ± 21.6 pA, n = 7, N = 3; “ns”, no significant difference, p = 0.7, unpaired Student’s t-test).